

1 **In situ chemical composition measurement of individual cloud residue**
2 **particles at a mountain site, South China**

3 Qin hao Lin^{1,2}, Guo hua Zhang¹, Long Peng^{1,2}, Xin hui Bi^{1,*}, Xin ming Wang¹, Fred J.
4 Brechtel³, Mei Li⁴, Duo hong Chen⁵, Ping'an Peng¹, Guo ying Sheng¹, Zhen Zhou⁴

5

6 ¹ State Key Laboratory of Organic Geochemistry and Guangdong Key Laboratory of
7 Environmental Protection and Resources Utilization, Guangzhou Institute of
8 Geochemistry, Chinese Academy of Sciences, Guangzhou, 510640, PR China

9 ² University of Chinese Academy of Sciences, Beijing, 100049, PR China

10 ³ Brechtel Manufacturing Inc., Hayward, 94544, California, USA

11 ⁴ Atmospheric Environment Institute of Safety and Pollution Control, Jinan University,
12 Guangzhou 510632, PR China

13 ⁵ State Environmental Protection Key Laboratory of Regional Air Quality Monitoring,
14 Guangdong Environmental Monitoring Center, Guangzhou 510308, PR China

15

16 * Correspondence to: Xinhui Bi (bixh@gig.ac.cn)

17 Tel.: +86-20-85290195

18

19 **Highlights**

- 20 1. EC-containing particles were the largest fraction of the total cloud residues (49.3% by
21 number), dominating in the range of 0.2-1.0 μm .
- 22 2. The Nf of the cloud residue types was influenced by air mass chemistry.
- 23 3. Amine particles represented from 0.2% to 15.1% by number of the total cloud residues
24 when air masses changed from northerly to southwesterly.
- 25 4. Compared with non-activated particles, nitrate intensity decreased in cloud residues
26 except dust type.

27 **Abstract**

28 To investigate how atmospheric aerosol particles interact with chemical composition of
29 cloud droplets, a ground-based counterflow virtual impactor (GCVI) coupled with a real-
30 time single-particle aerosol mass spectrometer (SPAMS) was used to assess the chemical
31 composition and mixing state of individual cloud residue particles in the Nanling
32 Mountain Range (1,690 m a.s.l.), South China, in Jan 2016. The cloud residues were
33 classified into nine particle types: Aged elemental carbon (EC), Potassium-rich (K-rich),
34 Amine, Dust, Pb, Fe, Organic carbon (OC), Sodium-rich (Na-rich) and Other. The largest
35 fraction of the total cloud residues was the Aged EC type (49.3% by number), followed
36 by the K-rich type (33.9% by number). Abundant Aged EC cloud residues that mixed
37 internally with inorganic salts were found in air masses from northerly polluted areas.
38 The number fraction (Nf) of the K-rich cloud residues increased within southwesterly air
39 masses from fire activities in Southeast Asia. When air masses changed from northerly
40 polluted areas to southwesterly ocean and livestock areas, the Amine particles increased
41 from 0.2% to 15.1% of the total cloud residues by number. The Dust, Fe, Pb, Na-rich and
42 OC particle types had a low contribution (0.5-4.1% by number) to the total cloud residues.
43 Higher fraction of nitrate (88-89% by number) was found in the Dust and Na-rich cloud
44 residues relative to sulfate (41-42%) and ammonium (15-23%). Higher intensity of nitrate
45 was found in the cloud residues relative to the ambient particles. Compared with non-
46 activated particles, nitrate intensity decreased in cloud residues except dust type. To our
47 knowledge, this study is the first report on in situ observation of the chemical
48 composition and mixing state of individual cloud residue particles in China.

49

50 Keywords: GCVI, SPAMS, cloud residues, mixing state, South China

51

52

53 **1 Introduction**

54 Aerosol-cloud interactions influence the thermodynamic and radiation balance of the
55 atmosphere (IPCC, Boucher et al., 2013). Anthropogenic particles can increase number
56 concentration of small cloud droplets, and, in turn, affect reflectivity and life time of
57 clouds (Stier et al., 2005; Lohmann et al., 2007; Rosenfeld et al., 2008). In situ cloud
58 chemical measurements have shown varied chemical composition of cloud water or
59 residues at various regions (Sorooshian et al., 2007a; Roth et al., 2016; Li et al., 2017).
60 Despite a large number of aerosol/cloud studies over the past 20 years, the uncertainty
61 for evaluating radiative forcing due to aerosol-cloud interactions has not been reduced
62 (Seinfeld. et al., 2016). Therefore, it is crucial to assess how atmospheric aerosol particles
63 contribute and interact with cloud droplets.

64 The ability of aerosol particles to act as cloud condensation nuclei (CCN) is dependent
65 on the size and chemical composition of particles at a given supersaturation (McFiggans
66 et al., 2006). Wiedensohler et al. (2009) found that the enhancement of particles CCN
67 ability was related to an increase in the average sulfate mass concentration. Dusek et al.
68 (2006) demonstrated that CCN behavior was more effected by aerosol size than chemical
69 composition. Meanwhile, aerosol mixing state also play an important role in the ability of
70 aerosol to act as CCN. It has been reported that freshly emitted elemental carbon (EC)
71 particles generally exhibit low CCN activity, whereas aged EC particles show high CCN
72 activity after experienced atmospheric processes (Zhang et al., 2008). Pratt et al. (2011)
73 found that number fractions of ammonium or oxalate internally mixed with biomass

74 burning particles increased with an aged time of 81-88 min, which promote CCN
75 behavior. Laboratory studies have shown that low-solubility organic particles internally
76 mixed with ammonium sulfate would suppress water uptake of mixed particle and thus
77 might affect CCN activity (Wise et al., 2003; Svenningsson et al., 2006; Sjogren et al.,
78 2007). An over prediction of CCN concentration by up to 35% was estimated based on
79 particle internal mixing state assumption (Medina et al., 2007; Collins et al., 2013). The
80 influence of mixing state on aerosol CCN activity varies depending on the proximity to
81 the pollution plume source and/or photochemical ageing activity (Ervens and Volkamer,
82 2010). More detailed measurements to characterize the mixing state of CCN particles
83 would improve our understanding of aerosol-cloud interactions.

84 The combined technique of a counterflow virtual impactor (CVI) and an Aerosol Mass
85 Spectrometer (AMS) or other online/offline single particle instruments is widely used to
86 characterize the chemical composition and/or mixing state of cloud/fog droplet residue
87 particles. These studies were mainly conducted in North America including Wyoming
88 (Pratt et al., 2010a), Ohio (Hayden et al., 2008), Oklahoma (Berg et al., 2009), Florida
89 (Cziczo et al., 2004; Twohy et al., 2005), California (Coggon et al., 2014), Europe
90 including Schmücke (Roth et al., 2016; Schneider et al., 2017), Jungfraujoch (Kamphus
91 et al., 2010), Åreskutan (Drewnick et al., 2007), Scandinavia (Targino et al., 2006),
92 Arctic (Zelenyuk et al., 2010), Central America (Cziczo et al., 2013), West Africa
93 (Matsuki et al., 2010) and marine areas (Twohy and Anderson 2008; Twohy et al., 2009;
94 Shingler et al., 2012).

95 Over the past three decades, China has undergone rapid economic growth accompanied
96 by increased aerosol emissions. Although scientists have worked to increase our

97 understanding of an emissions inventory and the temporal and spatial variation of
98 atmospheric aerosols in China (Zhang et al., 2012b), only few studies have employed
99 direct observation of the chemical composition and mixing state of cloud/fog droplets. Li
100 et al. (2011b) utilized transmission electron microscopy to obtain the mixing state of
101 individual ambient particles during cloud events at Mt. Tai in northern China. This result
102 showed that sulfate-related salts dominated in larger particles. Bi et al. (2016) used a
103 ground-counterflow virtual impactor (GCVI) coupled with a real-time single particle
104 aerosol mass spectrometer (SPAMS) to explore the chemical composition and mixing
105 state of individual fog residual particles at ground level in an urban area of South China.
106 They found an abundance of EC-containing particles in fog residues.

107 Here, we present a study on the chemical composition and mixing state of individual
108 cloud residue particles at a mountain site in South China. The same experimental
109 methods of Bi et al. (2016) were used in this study. The size distribution, chemical
110 composition and mixing state of cloud residues during cloud events are discussed.
111 Moreover, the chemical compositions of ambient and non-activated particles were also
112 compared with the cloud residues. The aim of this study is to assess the potential effects
113 of anthropogenic aerosols from regional transportation on cloud formation and to
114 investigate the dominant particle types in cloud droplets at a mountain site in South China.
115

116 **2 Experimental**

117 **2.1 Measurement site**

118 Our measurements were carried out during 15-26 Jan, 2016. The sampling site was
119 located in the Nanling Background Station (112 °53' 56" E, 24° 41' 56" N, 1,690 m a.s.l.)

120 at the National Air Pollution Monitoring System in South China (Figure S1). This station
121 is located at 200 km north of the metropolitan city Guangzhou and 350 km north of the
122 South China Sea (Figure S1). This site is also surrounded by a national park forest (273
123 km²), where there are scarcely any emissions from anthropogenic activities. During the
124 winter monsoon period, air pollution from northern China moves to southern China and
125 crosses the study region (Lee et al., 2005).

126

127 **2.2 Instrumentation**

128 In this study, a GCVI inlet system (GCVI Model 1205, Brechtel Mfg. Inc.) was used to
129 sample cloud droplets with a diameter greater than 8 μm . The ambient temperature on
130 average was 6.9 $^{\circ}\text{C}$ (ranging from -7.2 to 11.4 $^{\circ}\text{C}$) during cloud events. Only 20 cloud
131 residues that accounted for 0.08% of the total cloud residues were detected when the
132 ambient temperature was below -7 $^{\circ}\text{C}$ observed from 06:00 to 08:00 on 23 Jan. Thus,
133 cloud droplets were dominated by liquid water droplets. The measurements of the droplet
134 size spectra in this region performed during the winter of 1999-2001 showed that size of
135 cloud droplets ranged from 4 to 25 μm with average size of 10 μm and a corresponding
136 liquid water content of 0.11-0.15 g m^{-3} (Deng et al., 2007). Previous study in other
137 mountain site also showed an average size at ~ 10 μm (Borys et al., 2000). Hence,
138 assuming that size distribution of cloud droplets mostly was above 8 μm in this region.
139 The sampled cloud droplets were passed through an evaporation chamber (air flow
140 temperature at 40 $^{\circ}\text{C}$), where the associated water was removed and the dry residue
141 particles (with the air flow RH lower than 30%) remained. A stream of filtered and
142 heated ambient air (counterflow) was provided by a compressor. The particle

143 transmission efficiency of the cut size (8 μm) was 50%. The enrichment factor of the
144 particles collected by the GCVI inlet was estimated to be 5.25 based on theoretical
145 calculation (Shingler et al., 2012). Ambient particles were collected through an ambient
146 inlet with a cut-off aerodynamic diameter (d_a) of 2.5 μm when cloud-free periods were
147 present. Non-activated (interstitial) particles were sampled through the ambient inlet
148 during the cloud events in this study. The ambient or non-activated particles inlet was
149 dried using a silica gel diffusion dryer. During cloud-free periods, a ratio of particle
150 concentration measured behind the CVI (below 1 cm^{-3}) to ambient aerosol concentration
151 (2,000 cm^{-3}) was 0.0005, indicating that instances of particle breakthrough and small
152 particle contamination were absent. The cloud droplet residues, ambient or non-activated
153 particles were subsequently analyzed by a suite of aerosol measurement devices,
154 including a SPAMS (Hexin Analytical Instrument Co., Ltd., Guangzhou, China), a
155 scanning mobility particle sizer (SMPS) (MSP Cooperation) and an aethalometer (AE-33,
156 Magee Scientific Inc.).

157 A detailed operational principle of the SPAMS has been described elsewhere (Li et al.,
158 2011a). Briefly, aerosol particles are drawn into SPAMS through a critical orifice. The
159 particles are focused and aerodynamically sized by two continuous diode Nd:YAG laser
160 beams (532 nm). The particles are subsequently desorbed/ionized by a pulsed laser (266
161 nm) triggered exactly based on the velocity of the specific particle. The positive and
162 negative ions generated are recorded with the corresponding size of individual particles.
163 Polystyrene latex spheres (Nanosphere Size Standards, Duke Scientific Corp., Palo Alto)
164 of 0.2-2.0 μm in diameter were used to calibrate the sizes of the detected particles. The
165 ambient pressure was 830 hPa (826-842 hPa) during the measurements and the

166 calibration. Particles measured by SPAMS mostly fell within the size range of d_{va} 0.2-2.0
167 μm (Li et al., 2011a).

168

169 **2.3 Definition of cloud events**

170 To reliably identify the presence of cloud events, an upper-limit visibility threshold of 5
171 km and a lower-limit relative humidity (RH) threshold of 95% were set in the GCVI
172 software (Bi et al., 2016). Three long-lasting cloud events occurred during the periods of
173 16:00 (local time) 15 Jan - 07:00 17 Jan (cloud I), 20:00 18 Jan - 12:00 19 Jan (cloud II)
174 and 17:00 19 Jan - 13:00 23 Jan (cloud III), as marked in Figure 1. In addition, a cloud
175 event occurred at 14:40 - 15:00 on 17 Jan, but we did not do an analysis due to the short
176 duration. The measured cloud residual concentration was integrated by the SMPS and
177 was then corrected by the enrichment factor and transmission efficiency of the GCVI.
178 The corrected cloud residual concentrations on average were 436 cm^{-3} , 568 cm^{-3} and 544
179 cm^{-3} for cloud I, cloud II and cloud III, respectively (Figure S2). From 10:00 21 Jan to
180 13:00 23 Jan, cloud residues and non-activated particles were alternately sampled with an
181 interval of one hour. During this period, a ratio of number residues to total number
182 particles (sum of cloud residues and non-activated particle) on average was 0.43 ± 0.20 .
183 Low levels of $\text{PM}_{2.5}$ ($\sim 12.7\text{ }\mu\text{g m}^{-3}$) exclude the influence of hazy days. A rainfall
184 detector of the GCVI system was also used to exclude rain droplet contamination. When
185 cloud events occurred without precipitation, sampling was automatically triggered by the
186 GCVI control software (Bi et al., 2016).

187

188

189 **2.4 Particle classification**

190 During this study period, a total of 73,996 particles including 49,322 ambient, 23,611
191 cloud residual and 1,063 non-activated particles with bipolar mass spectra were
192 chemically analyzed in the size range of d_{va} 0.2-1.9 μm . The sampled particles were
193 firstly classified into 101 clusters using an Adaptive Resonance Theory neural network
194 (ART-2a) with a vigilance factor of 0.75, a learning rate of 0.05, and 20 iterations (Song
195 et al., 1999). Then by manually combining similar clusters, eight major particle types
196 Aged EC, Potassium-rich (K-rich), Amine, Dust, Fe, Pb, Organic carbon (OC), and
197 Sodium-rich (Na-rich) with distinct chemical patterns were obtained, which represented
198 ~99.9% of the population of the detected particles. The remaining particles were grouped
199 together as “Other”. Assuming that the number of individual particles followed Poisson
200 distribution, standard errors for number fraction of particle type were estimated (Pratt et
201 al., 2010a).

202

203 **3 Results and discussion**

204 **3.1 Back trajectories and meteorological conditions**

205 Back trajectories in this study were calculated using the Hybrid Single Particle
206 Lagrangian Integrated Trajectory (HYSPLIT Model). A height of the HYSPLIT model in
207 the study region (a spatial resolution of $0.5^\circ \times 0.5^\circ$) is averaged 500 m a.s.l., lower than
208 height of the observed site (1,690 m a.s.l.). Thus, a height of 1,800 m a.s.l.
209 (approximately 100 m above the observed site) was chosen as an endpoint in the model.
210 The station was mainly affected by southwesterly or northerly air masses in this study
211 (Figure 2). In addition, the beginning altitude of the southwesterly air masses traversed at

212 lower heights relative to the northerly air masses (Figure 2). The southwesterly air masses,
213 accompanied by warm moist airflows, occurred during 15-17 and 20-21 Jan, which
214 promoted high RH condition (Figure 1). Conversely, the northerly air masses, associated
215 with cool dry airstreams, occurred during 18 and 23-24 Jan and led to a decrease in
216 temperature and relative humidity. Note that, on 18-19 and 22-23 Jan, the air mass
217 encountered initial mixing of northerly cloud-free air and southwesterly cloudy air.
218 Entrainment of nuclei particles originated from northern air masses might be activated to
219 cloud droplets (Sect. 3.4).

220 Meteorological conditions were unstable, with high southwesterly flow ($\sim 6.5 \text{ m s}^{-1}$)
221 during 15-17 and 20-22 Jan (Figure 1). The level of $\text{PM}_{2.5}$ remained a low value of
222 approximately $3 \mu\text{g m}^{-3}$ for this time period. A high level of $\text{PM}_{2.5}$ ($\sim 20 \mu\text{g m}^{-3}$) was
223 observed during 18 Jan when the northerly flow dominated. Similarly, the average $\text{PM}_{2.5}$
224 value reached $24 \mu\text{g m}^{-3}$ during 24 Jan. Although the local northerly and southwesterly
225 flows occurred alternately, the particles were still originated from the northerly air mass
226 for this period (Figure 2). During 23-24 Jan, a sharp decrease in temperature (Figure 1)
227 was observed due to a cold wave associated with a violent northerly flow. The wind
228 speed during the cold wave exceeded the upper-limit speed ($\sim 12 \text{ m/s}$) of a wind speed
229 sensor.

230

231 **3.2 The chemical characterization of cloud droplet residues**

232 Figure 3 shows the average positive and negative mass spectra of the main six particle
233 types. The Aged EC particles were characterized by EC cluster ions (e.g., $m/z \pm 12\text{C}^{+/-}$,
234 $\pm 36\text{C}_3^{+/-}$, $\pm 48\text{C}_4^{+/-}$, $\pm 60\text{C}_5^{+/-}$, ...) and a strong K^+ ion signal ($m/z 39\text{K}^+$) as well as a

235 sulfate ion signal (m/z -97HSO₄⁻), and some minor organic markers (m/z 27C₂H₃⁺,
236 43C₂H₃O⁺) (Moffet and Prather, 2009). EC particles mainly originated from combustion
237 processes (Bond et al., 2013). The strong K⁺ ion signal in the Aged EC particles implies
238 partially originated from biomass burning sources (Bi et al. 2011). The Aged EC particle
239 type was the largest fraction (49.3% by number) of the total cloud residues (Figure S3).
240 In addition, number fraction (Nf) of the Aged EC residues significantly decreased from
241 54.1% in the size range of 0.2-1.0 μm to 19.2% in the size range of 1.1-1.9 μm (Figure 4).
242 Note that the chemical composition of cloud residues is dependent on the particle size
243 (Roth et al., 2016), and the number reported for each particle type might suffer from the
244 bias related to size-dependent transmission efficiency (Qin et al., 2006). The relative
245 fraction of cloud residues in 0.1 μm size interval is presented to minimize the influence of
246 size-dependent transmission efficiency of single particle mass spectrometry (Roth et al.,
247 2016).

248 The K-rich particles exhibited the highest peak at m/z 39K⁺, mainly combined with
249 sulfate and nitrate (m/z -46NO₂⁻, -62NO₃⁻) and presumably derived from biomass/biofuel
250 burning source (Moffet et al., 2008; Pratt et al. 2011; Zhang et al., 2013). An aged time
251 of 81-88 min biomass burning particles were found to show an increase in the mass
252 fractions of ammonium, sulfate, and nitrate (Pratt et al. 2011). In this study, the K-rich
253 particles would be expected to experience aged process due to strong sulfate and nitrate
254 signals (Hudson et al. 2004; Pratt et al. 2011). Aged biomass burning particles can
255 participate in cloud droplets formation and show an effective CCN activity (Pratt et al.
256 2010a). The K-rich particle type, the second largest contributor, accounted for 33.9% by
257 number of the total cloud residues (Figure S3).

258 The abundant aged soot/EC and biomass burning particles were often detected in
259 cloud residues (Pratt et al., 2010a; Roth et al., 2016). The contribution of local
260 anthropogenic origins to aged soot and/or biomass burning particles in cloud/fog residues
261 has been reported in Schmücke (Roth et al., 2016) and Guangzhou city (Bi et al., 2016).
262 At the North Slope of Alaska, the measurement of biomass burning particles in cloud
263 residues mainly resulted from local vicinity or as far away as Siberia and Asian sources
264 (Zelenyuk et al., 2010; Hiranuma et al., 2013). Similarly, the majority of Aged EC and K-
265 rich cloud residues observed here are expected to originate from long-range
266 transportation due to insignificant sources of local anthropogenic emissions and the fire
267 dots (Figure 2). At the Jungfrauoch station (3,580 m a.s.l.) in Europe, the K-rich
268 (biomass burning) particles only contributed 3% of the cloud droplets, and the Aged EC
269 residuals were insignificant (<1% by number) (Kamphus et al., 2010). The Jungfrauoch
270 station is predominantly within the free tropospheric condition, such that the biomass
271 burning contribution can be expected to be lower than at other sites.

272 The Amine particles were characterized by related amine ion signals at m/z
273 $58\text{C}_2\text{H}_5\text{NHCH}_2^+$ (diethylamine, DEA), $59\text{N}(\text{CH}_3)_3^+$ (trimethylamine, TMA) and
274 $86\text{C}_5\text{H}_{12}\text{N}^+$ (triethylamine, TEA) (Angelino et al., 2001; Moffet et al., 2008). This
275 particle type also contained sulfuric acid ion signals at m/z $-195\text{H}(\text{HSO}_4)_2^-$, indicative of
276 acidic particles (Rehbein et al., 2011). The Amine particles represented 3.8% by number
277 of the total cloud residues (Figure S3). Higher N_f of the Amine residues was detected in
278 the size range from 0.7 to 1.9 μm relative to the size range from 0.2 to 0.6 μm (16.7%
279 versus 0.4%), as shown in Figure 4. Aqueous reactions improving the participation of
280 amine have been observed in Guangzhou (Zhang et al., 2012a) and Southern Ontario

281 (Rehbein et al., 2011). A recent study also showed a clear enhancement of amine-
282 containing particles in cloud residues compared to the ambient particles (9% versus 2%
283 by number) (Roth et al., 2016). It indicates a preferential formation of amine within the
284 cloud, which is in contrast to the observations of Bi et al. (2016). It might suggest that
285 enhancement of particle amine is not only depend on high RH or fog/cloud process, but
286 also sensitive to other parameters, such as presence of gas phase amine source (Rehbein
287 et al., 2011).

288 The Dust particles presented significant ions at m/z 40Ca^+ , $56\text{CaO}^+/\text{Fe}^+$, $96\text{Ca}_2\text{O}^+$
289 and -76SiO_3^- and sulfate as well as nitrate markers. Previous studies showed that dust
290 particles that are internally mixed with sulfate and nitrate are expected to act as CCN
291 (Twohy and Anderson 2008; Twohy et al., 2009), despite sulfate and nitrate partially
292 forming from in-cloud production. This type contributed 2.9% by number of the total
293 cloud residues (Figure S3). A slight increase in Nf of the Dust residues was observed in
294 size range above $0.5\ \mu\text{m}$ relative to that below $0.5\ \mu\text{m}$ (3.0% versus 1.0% by number). At
295 Mt. Tai in northern China, a high concentration of Ca^{2+} in cloud/fog water was mainly
296 attributed to a sandstorm event during the spring season (Wang et al., 2011). At Mt. Heng
297 in southern China, the abundant crust-related elements (e.g., Al) observed in cloud water
298 is due to Asian dust storms that occurred in March-May (Li et al., 2017). Based on the
299 backward trajectory, the site was unlikely affected by sandstorm source in northwestern
300 China during the cloud events. Local dust emissions by anthropogenic-disturbing soils or
301 removing vegetation cover can be excluded as a result of forest protection. Additionally,
302 dust residues may have occupied larger CCN (Tang et al., 2016), which cannot be

303 detected by the SPAMS. Hence, a low fraction (2.9% by number) of dust cloud residue
304 might be due to the limitation of the SPAMS.

305 The Fe particles had its typical ions at m/z 56Fe^+ and internally mixed with sulfate
306 and nitrate, made up 4.1% by number of the total cloud residues. Approximately 16% of
307 the Fe cloud residues contained Ca^+ peak (m/z 40). Predominant Fe ion peaks possibly
308 indicates the contribution from anthropogenic sources (Zhang et al., 2014), especially the
309 northern air masses across iron/steel industrial activities in Yangtze River Mid-Reaches
310 city clusters (Figure 2). The contribution of anthropogenic and natural Fe-containing
311 particles sources (Moteki et al., 2017) to observed Fe-containing residues is expected.
312 The presence of Fe in the cloud droplets play an important role in aqueous-phase SO_2
313 catalytic oxidation in cloud processing (Harris et al., 2013), thus accelerating the sulfate
314 content of Fe-containing particles in cloud processing.

315 The Na-rich particles were mainly composed of ion peaks at m/z 23Na^+ and 39K^+ in
316 the positive mass spectra, and nitrate and sulfate species in the negative mass spectra,
317 made up 3.0% by number of the total cloud residues. Na-rich particles are formed from
318 varied sources including industrial emissions, sea salt or dry lake beds (Moffet et al.
319 2008). The Nf of Na-rich cloud residues did not increase from continental (Northerly) air
320 mass on 19 Jan to maritime (southwesterly) air mass on 21 Jan (3.3% versus 2.4% by
321 number). However, the related sea salt ion peak area (m/z , $81/83 \text{Na}_2^{35}\text{Cl}^+/\text{Na}_2^{37}\text{Cl}^+$) were
322 enhanced for Na-rich particles origination from maritime air mass relative to continental
323 air mass (3.8 ± 2.4 times). The continental air masses crossed industrial areas where the
324 Yangtze River Mid-Reaches city cluster is located (Figure 2). Industrial emissions were a
325 possible contributor to Na-rich particles under the influence of continental air masses

326 (Wang et al. 2016). This might suggest that the Na-rich particles were originated from
327 both industrial emissions and sea salts.

328 The OC, Pb and Other particle types contributed 0.1%-2.3% by number to the total
329 cloud residues (Figure S3). Their average mass spectra can be found in Figure S4. The
330 OC particles presented dominant intense OC signals (e.g., m/z $27C_2H_3^+$, $37C_3H^+$,
331 $43C_2H_3O^+$ and $51C_4H_3^+$) and abundant sulfate. Presence of K^+ signal was found in the
332 OC particles, suggesting possible biomass burning sources (Bi et al. 2011). OC particles
333 might exist in smaller cloud residues (Sellegri et al., 2003a), which cannot be detected by
334 the SPAMS. The Pb particles showed its typical ions at m/z $208Pb^+$ and internally mixed
335 with K^+ and Cl^- . Previous studies have found that K and Cl internally mixed with Pb
336 particles have a possible origination of waste incineration (Zhang et al., 2009) or iron and
337 steel products manufacturing facilities (Tsai et al., 2007). Only three particles were found
338 containing calcium, organic carbon, organic nitrogen and phosphate ion signals, implying
339 a possible existence of biological particles (Pratt et al., 2009a). Such particles were
340 classified as the Other type due to low number.

341 Previous measurements have found that dust, playa salts, sea salt or metal particles
342 were often enriched in larger cloud droplets ($\sim 20 \mu m$) (Bator and Collett, 1997; Moore et
343 al., 2004; Pratt et al., 2010b). Organic carbon tended to be enriched in small cloud/fog
344 droplets, extending to $4 \mu m$ (Herckes et al., 2013). The size of cloud droplets were above
345 $8 \mu m$ in the present study. Additionally, the particle transmission efficiency increased
346 with increasing cloud droplet size (Shingler et al., 2012). Thus, it partially leads to
347 relatively larger fractions of the observed Dust, Na-rich and metal cloud residues, and the
348 less fraction of the OC cloud residues in this study.

349 **3.3 Mixing state of secondary species in cloud residues**

350 The high Nfs of sulfate-containing particles were found in the K-rich (91%), OC (100%),
351 Aged EC (98%), Pb (74%), Fe (93%) and Amine (99%) cloud residues, as shown in
352 Figure 5. Lower Nfs of sulfate-containing particles were observed in the Na-rich (41%)
353 and Dust (42%) cloud residues. In contrast, nitrate-containing particles contributed 89%
354 and 88% by number to the Na-rich and Dust cloud residues, respectively. The acid
355 displacement reaction of sea salt chloride (Na-rich particles) by HNO₃ might lead to a
356 depletion of chloride and enhancement of nitrate (Laskin et al., 2012). Similarly, the
357 heterogeneous chemistry of HNO₃ in the dust particles also contributes the preferential
358 enrichment of nitrate (Tang et al., 2016). Moreover, after activation, uptake of gas-phase
359 HNO₃ would increase nitrate level in the cloud residues (Schneider et al., 2017). The
360 nitrate in the cloud residues was thought to be in the form of ammonium nitrate by
361 estimating the ratio of m/z 30 to m/z 46 in AMS data (Drewnick et al., 2007; Hayden et
362 al., 2008). Relative to nitrate, low portions of ammonium (m/z, 18NH₄⁺) in the Na-rich
363 (23% by number) and Dust (15% by number) cloud residues suggest that in this region,
364 ammonium nitrate was not a predominant form of nitrate in the two cloud residual types.
365 The Na-rich and Dust types were mainly composed of alkaline ion peaks (m/z, 23Na⁺,
366 39K⁺ and 40Ca⁺) in position mass spectra (Figure 3), accompanied with larger fraction
367 (88-89%) of nitrate. Thus, our data suggests that nitrate might exist in the form of
368 Ca(NO₃)₂, NaNO₃ or KNO₃ in the Dust and Na-rich cloud residues. It should be noted
369 that the evaporation chamber of the GCVI may lead to a reduction of ammonium nitrate
370 in the cloud residues (Hayden et al., 2008). The nitrate-containing particles accounted for
371 only 46% by number of the Aged EC cloud residues, which is significantly less than the

372 sulfate-containing particles. Previous field studies have found that Aged EC (soot)
373 fog/cloud residues are mainly internally mixed with sulfate (Pratt et al., 2010a; Harris et
374 al., 2014; Bi et al., 2016). Aged EC particles mixed with sulfate are good CCN, rather
375 than formed by in-cloud processing (Bi et al., 2016; Roth et al., 2016). Laboratory
376 measurements have also demonstrated that EC particles internally mixed with sulfate
377 showed a high hygroscopic behavior and thus affect CCN ability (McMeeking et al.,
378 2011). High portions (75-86% by number) of ammonium-containing particles were
379 observed for the OC and Aged EC cloud residues, suggesting that ammonium will mostly
380 be in the form of ammonium sulfate or ammonium nitrate for two cloud residual types
381 (Zhang et al., 2017). This result also implies that ammonium-containing particles are
382 preferentially activated or enhanced uptake of gaseous NH_3 to neutralize acidic cloud
383 droplets for the OC and EC types.

384 Water soluble organics (e.g., amine and oxalate) have previously been measured in
385 cloud water/residues (Sellegri et al., 2003b; Sorooshian et al., 2007a; Pratt et al., 2010a).
386 The presence of TMA (93% by number) in the Amine cloud residues is expected to
387 promote water uptake activity (Sorooshian et al., 2007b). A total of 3,410 oxalate-
388 containing particles (m/z , $-89\text{HC}_2\text{O}_4^-$) represented 14.4% by number of the total cloud
389 residues, which was mainly associated with the K-rich cloud residues (~70% by number).
390 Oxalate-containing particles (~30% by number) in the metal (Pb, Fe) cloud residues
391 might be in the form of metal oxalate complexes from reactions of in-cloud formation
392 oxalate with metals (Furukawa and Takahashi, 2011). Oxalate can readily partition into
393 the particle phase to form amine salts (Pratt et al., 2009b). It may facilitate the
394 entrainment of oxalate (33% by number) in the Amine residues. A low fraction (4%) of

395 oxalate-containing particles in the OC type is a result of restrictive classification.
396 Classification of the OC particles is mainly based on intense organic carbon ion signals
397 (e.g., m/z $27C_2H_3^+$, $37C_3H^+$, $43C_2H_3O^+$ and $51C_4H_3^+$). The majority of oxalate-containing
398 particles were internally mixed with the K-rich type. Therefore, oxalate was classified to
399 the K-rich type and probably contributed from biomass burning. The K-rich particles
400 could contain an abundance of organics (Pratt et al. 2011), however, the signals of
401 organics were covered by the potassium due to its high sensitivity to the laser.

402

403 **3.4 Comparison of cloud residues in different air mass sources**

404 Figure 6 displays the hourly detected particle counts and Nf values of the nine types of
405 cloud residues and ambient particles. The Nf of the Aged EC type showed a very abrupt
406 increase from cloud residues to ambient particles on Jan 17. The ambient RH showed an
407 abrupt decrease from nearly 100% at 10:00 to 85% at 11:00 on 17 Jan (Figure 1). The
408 ambient temperature also decreased from 10 °C at 11:00 to 4 °C at 18:00 on 17 Jan
409 (Figure 1). These changes imply that the air mass shifted from southwesterly cloudy air
410 to northerly cloud-free air around noon on 17 Jan (Figure 2). The entrained particles
411 originated from northern air mass might have insufficient supersaturation to be activated
412 as cloud droplets. It resulted in the remarkable increase of the Aged EC particles in
413 ambient particles on Jan 17 (Figure 6).

414 The ambient RH increased from 60% at 19:00 to nearly 100% at 21:00 on 18 Jan
415 (Figure 1). The ambient temperature also increased from 1.3 °C at 22:00 on 18 Jan to
416 3.2 °C at 06:00 on 19 Jan (Figure 1). These changes imply that the air mass changed from
417 northerly cloud-free air to southwesterly cloudy air at night on 18 Jan (Figure 2). During

418 18-19 Jan, the cloud residues and ambient particles showed similar chemical
419 characteristics and were dominated by Aged EC particles (Figure 6). A lack of significant
420 variation in the particle types for this period suggests that nuclei particles originated from
421 northerly cloud-free air could be activated to become cloud droplets. When a cloud-free
422 event occurred at 11:00-17:00 on 19 Jan, ambient particles remained a high level of $\text{PM}_{2.5}$
423 ($\sim 22.7 \mu\text{g m}^{-3}$). The southwesterly wind flow on 19-20 Jan was too weak ($\sim 2.75 \text{ m s}^{-1}$)
424 to dilute particles originated from the northerly air masses (Figure 1). Additionally, a
425 high RH (90%) air mass at height 1,500 m (a.s.l.) gradually moved to northern China
426 from 19 to 20 Jan (Figure S5). These changes might have led to similar residual particle
427 types observed from 19 Jan to 20 Jan, although the site encountered southwesterly cloudy
428 air on 19-20 Jan (Figure 2).

429 As mentioned above, the Nf of the cloud residue types significantly changed as the
430 air mass origin varied from northerly to southwesterly. To further investigate the
431 influence of air mass history, we selected to analyze cloud residues that had arrived from
432 a northerly air mass on 18-19 Jan as compared to cloud residues that originating from a
433 southwesterly air mass during the periods of 16-17 and 21-22 Jan. The detected number
434 of cloud residues for both the northerly and southwesterly air masses are given in Table
435 S1. The southwesterly air masses accompanied by high relative humidity (90%) (Figure
436 S5) may have triggered particles activated to CCN prior to their arrival to the sampling
437 site.

438 The K-rich type was found to contribute 23.9% to the cloud residues in the northerly
439 air mass, which was significantly lower than its contribution to the southwesterly air mass
440 (51.5%), as shown in Figure 7. A similarity in averaged mass spectrum of the K-rich

441 residues was found for the southwesterly and northerly air masses (Figure S6). The
442 considerable increase of K-rich cloud residues suggests a major influence of regional
443 biomass-burning activities. Biomass-burning emissions from Southeast Asia, including
444 Myanmar, Vietnam, Laos and Thailand, where abundant fire dots are observed (Figure 2),
445 could have been transported to the sampling site under a southwesterly air mass (Duncan
446 et al., 2003). In contrast, the Aged EC type represented only 23.7% of the cloud residues
447 under the influence of the southwesterly air mass, which was significantly lower than
448 observations for the northerly air mass (59.9%), as shown in Figure 7. This result
449 suggests that the northern air mass has a greater influence on the presence of Aged EC
450 cloud residues.

451 An obvious increase in Nf of the Amine type was observed in the southwesterly air
452 mass (15.1%) compared to the northerly air mass (0.2%), as shown in Figure 7. This data
453 implies that the sources or formation mechanisms of amine in cloud residues varied in
454 different air masses. The southwesterly air masses arrived from as far as the Bay of
455 Bengal and then travelled through Southeast Asia region before reaching South China
456 (Figure 2). The potential gas amine emissions from ocean (Facchini et al., 2008) and
457 livestock areas (90 million animals, data was available at the website
458 <http://faostat3.fao.org>) in Southeast Asia region might promote the enrichment of amine
459 particles. Furthermore, after activation, the partitioning of the gas amine on cloud
460 droplets may further contribute to the enhanced Amine cloud residues (Rehbein et al.,
461 2011), especially for air masses delivered via routes with high relative humidity, as
462 mentioned above (Figure S5). In contrast, northerly air mass accompanied with dry

463 airstreams may unfavorably induce the partitioning of gas amines into the particle phase
464 (Rehbein et al., 2011).

465

466 **3.5 Comparison of cloud residues with ambient and non-activated particles**

467 A direct comparison between cloud residues and ambient particles was limited because of
468 their differences in air mass origins. During the sampling period, the cloud events
469 occurred once the southwesterly air masses were dominant. Hence a comparison between
470 cloud residues and ambient particles cannot be addressed under the influence of
471 southwesterly air masses. Here, we chose five hours before and after the beginning of the
472 cloud II period in order to compare cloud residues and ambient particles with similar
473 northerly air mass origins, as discussed in Sect. 3.4.

474 The cloud residues and non-activated particles were alternately sampled with an
475 interval of one hour from 21 Jan to 23 Jan. The ambient temperature decreased from 6 °C
476 at 11:00 to 0 °C at 23:00 on 22 Jan (Figure 1). Ambient particles level (sum of residual
477 and non-activated particles) showed a clearly increase from 156 cm⁻³ to 1460 cm⁻³ during
478 this period (Figure S2). Thus, the data suggests that the initial mixing of northerly cloud-
479 free air and southwesterly cloudy air occurred around noon on 22 Jan. A reduction of
480 supersaturation due to entrainment of the dry northern air mass might have insufficient
481 moisture to activate small particles, leading to unactivated particles above 0.2 μm
482 (Figure S7) (Mertes et al., 2005; Kleinman et al., 2012; Hammer et al., 2014), which can
483 be detected by the SPAMS.

484 The contribution of K-rich particles in cloud residues (23.9%) slightly decreased
485 relative to ambient particles (30.7%), as shown in Figure 7. Previous studies have found

486 that there were no significant changes in Nf of biomass-burning particles for cloud
487 residues relative to ambient particles (Pratt et al., 2010a; Roth et al., 2016). The biomass-
488 burning particles internally mixed with soluble species (e.g., sulfate, nitrate and oxalate)
489 enhanced their ability to act as CCN, as discussed in Sect. 3.3. Kamphus et al. (2010)
490 reported that biomass-burning particles account for only 3% of cloud residues compared
491 with 43% of ambient particles, and they suspected that biomass-burning particles might
492 exist in the form of tar balls (hydrophobic materials). A slight increase in Nf of the Aged
493 EC cloud residues (59.9%) was observed relative to ambient particles (53.8%), as shown
494 in Figure 7. In general, freshly emitted EC particles are less hydrophilic and are not
495 active as CCN (Bond et al., 2013). The Aged EC particles show a high degree of internal
496 mixing with secondary inorganic compounds in this study (Figure 5), improving their
497 ability to act as CCN. The remaining particle types showed no clear differences in Nf
498 between cloud residues and ambient particles.

499 When comparing the cloud residues with non-activated particles, a significant change
500 in Nf was found for the Aged EC and K-rich type. A higher Nf of K-rich particles and a
501 lower Nf of EC particles were found for the cloud residues relative to the non-activated
502 particles (Figure 7). Entrainment of northerly cloud-free air might lower supersaturation
503 during this period. Aged EC particles may require very high supersaturation to grow into
504 cloud droplets and thus, only form hydrated non-activated aerosol (Hallberg et al., 1994).

505 Figure 8 and 9 show the differences in average mass spectra for cloud residues
506 versus ambient particles, as well as cloud residues versus non-activated particles,
507 respectively. Nitrate intensity (average ion peak area) enhanced in the cloud residues
508 when compared to ambient particles. In addition, nitrate-containing particles accounted

509 for 70% of the cloud residues compared to 38% of the ambient particles. Drewnick et al.
510 (2007) suggested that rather than sulfate, high nitrate content in pre-existing particles
511 preferentially acted as cloud droplets. Compared with nitrate-containing ambient particles,
512 larger size of containing-nitrate residues (Figure S8) possibly reflect the uptake of
513 gaseous HNO₃ during cloud process (Hayden et al. 2008; Roth et al., 2016). A recent
514 study also confirmed that the uptake of gaseous HNO₃ is an important contributor for the
515 increased nitrate level in the cloud residuals (Schneider et al., 2017). Interestingly, we
516 observed a decrease in nitrate intensity in cloud residues except dust type (Figure 9), and
517 a large size distribution of nitrate-containing cloud residues (Figure S7) when compared
518 with non-activated particles. This result suggests that particle size, rather than nitrate
519 content, plays a more important role in the activation of particles into cloud droplets.

520 Sulfate intensity enhancement was only observed in the OC cloud residues relative to
521 both ambient and non-activated particles. Although the in-cloud addition of sulfate can be
522 produced from aqueous Fe-catalyzed or oxidation by H₂O₂/O₃ reactions (Harris et al.,
523 2014), sulfate abundance was found in the Fe cloud residues relative to non-activated
524 particles, but no enhancement relative to ambient particles. Previous studies also showed
525 that the mass or number fraction of sulfate-containing particles in the cloud residues
526 changed between ambient and non-activated particles (Drewnick et al., 2007; Twohy and
527 Anderson, 2008; Schneider et al., 2017). However, the reason for these changes remains
528 unclear.

529 The in-cloud process has been reported to be an important pathway for the production
530 of amine particles (Rehbein et al., 2011; Zhang et al., 2012a). In this study, no
531 remarkable change in Nf of the Amine cloud residues was obtained relative to the

532 ambient particles (0.2% versus 0.2% by number), as shown in Figure 7. The absence of
533 amine species in cloud residues may be partially affected by droplet evaporation in the
534 GCVI (Bi et al., 2016). However, there was a high fraction of the amine cloud residuals
535 when the southwesterly air mass prevailed, as discussed in Sect. 3.4. A lack of gas-phase
536 amines may be the cause of few amine particles detected in the ambient particles and
537 cloud residues (Rehbein et al., 2011). An increase in Nf of cloud residues was observed
538 compared with non-activated particles (5.2% versus 0.1% by number), as shown in
539 Figure 7. An increase of particle water content facilitates partitioning of gas-phase amine
540 species into the aqueous phase when gas-phase amines present (Rehbein et al., 2011).

541

542 **4 Conclusions**

543 This study presented an in situ observation of individual cloud residues, non-
544 activated and ambient particles at a mountain site in South China. The finding shows that
545 the Aged EC (49.3%) and K-rich types (33.9%) dominate the cloud residues in a remote
546 area of China, followed by the Fe (4.1%), Amine (3.8%), Na-rich (3.0%) and Dust (2.9%)
547 types. The OC, Pb and Other types contributed 0.1%-2.3% by number to the total cloud
548 residues. The observed change in Nf of the cloud residue types, influenced by various air
549 masses, highlights the important role of regional transportation in the observed cloud
550 residual chemistry. Amine particles represented from 0.2% to 15.1% by number of the
551 total cloud residues dependent on the air mass history. Sulfate was found to be highly
552 mixed with the K-rich, OC, Aged EC, Pb, Fe and Amine cloud residues, while nitrate was
553 highly mixed with the Na-rich and Dust cloud residues. Compared with non-activated
554 particles, nitrate intensity decreased in cloud residues except dust type, and sulfate

555 intensity enhancement was only observed in the OC and Fe cloud residues.

556

557 **Acknowledgments**

558 This work was supported by the National Key Research and Development Program of
559 China (2017YFC0210100), the National Nature Science Foundation of China (No.
560 91544101 and 41405131) and the Foundation for Leading Talents of the Guangdong
561 Province Government. The authors thank Ji Ou from Shaoguan city Environmental
562 Monitoring Center for the help during the study. We also acknowledge the NOAA Air
563 Resources Laboratory (ARL) for the provision of the HYSPLIT transport and dispersion
564 model and/or READY website (<http://ready.arl.noaa.gov>) used in this publication. All the
565 data can be obtained by contacting the corresponding author.

566

567 **References**

568 Angelino, S., Suess, D.T. and Prather, K. A.: Formation of aerosol particles from
569 reactions of secondary and tertiary alkylamines: Characterization by aerosol time-of-
570 flight mass spectrometry, *Environ. Sci. Technol.*, 35, 3130-3138, doi:
571 10.1021/es0015444, 2001.

572 Bator, A. and Collett, J.L.: Cloud chemistry varies with drop size, *J. Geophys. Res.*
573 *Atmos.*, 102, 28071-28078, 1997.

574 Bi, X., Lin, Q., Peng, L., Zhang, G., Wang, X., Brechtel, F. J., Chen, D., Li, M., Peng, P.
575 a., Sheng, G. and Zhou, Z.: In situ detection of the chemistry of individual fog droplet
576 residues in the Pearl River Delta region, China, *J. Geophys. Res. Atmos.*, 121(15),
577 9105-9116, doi:10.1002/2016jd024886, 2016.

578 Bi, X., Zhang, G., Li, L., Wang, X., Li, M., Sheng, G., Fu, J. and Zhou, Z.: Mixing state
579 of biomass burning particles by single particle aerosol mass spectrometer in the urban
580 area of PRD, China. *Atmos. Environ.*, 45, 3447-3453,
581 doi:10.1016/j.atmosenv.2011.03.034, 2011.

582 Berg, L.K., Berkowitz, C.M., Hubbe, J.M., Ogren, J.A., Hostetler, C.A., Ferrare, R.A.,
583 Hair, J.W., Dubey, M.K., Mazzoleni, C. and Andrews, E.: Overview of the cumulus
584 humilis aerosol processing study, *B. Am. Meteorol. Soc.* 90, 1653-1667,
585 <http://dx.doi.org/10.1175/2009BAMS2760.1>, 2009.

586 Bond, T. C., Doherty, S. J., Fahey, D. W., Forster, P. M., Berntsen, T., DeAngelo, B. J.,
587 Flanner, M. G., Ghan, S., Krächer, B., Koch, D., Kinne, S., Kondo, Y., Quinn, P. K.,
588 Sarofim, M. C., Schultz, M. G., Schulz, M., Venkataraman, C., Zhang, H., Zhang, S.,
589 Bellouin, N., Guttikunda, S. K., Hopke, P. K., Jacobson, M. Z., Kaiser, J. W., Klimont,
590 Z., Lohmann, U., Schwarz, J. P., Shindell, D., Storelvmo, T., Warren, S. G. and Zender,
591 C. S.: Bounding the role of black carbon in the climate system: A scientific assessment,
592 *J. Geophys. Res. Atmos.*, 118, 5380-5552, doi:10.1002/jgrd.50171, 2013.

593 Borys, R. D., Lowenthal, D. H. and Mitchell, D. L.: The relationships among cloud
594 microphysics, chemistry, and precipitation rate in cold mountain clouds, *Atmos.*
595 *Environ.*, 34(16), 2593-2602, 2000.

596 Boucher, O., Randall, D., Artaxo, P., Bretherton, C., Feingold, G., Forster, P., Kerminen,
597 V., Kondo, Y., Liao, H., Lohmann, U., Rasch, P., Satheesh, S., Sherwood, S., Stevens,
598 B. and Zhang X.: Clouds and Aerosols. In *Climate Change 2013: The Physical Science*
599 *Basis. Contribution of Working Group I to the Fifth Assessment Report of the*
600 *Intergovernmental Panel on Climate Change* [Stocker, T.F., D. Qin, G.-K. Plattner, M.

601 Tignor, S.K. Allen, J. Boschung, A. Nauels, Y. Xia, V. Bex and P.M. Midgley (eds.)].
602 Cambridge University Press, Cambridge, United Kingdom and New York, NY, USA.
603 2013.

604 Coggon, M.M., Sorooshian, A., Wang, Z., Craven, J.S., Metcalf, A.R., Lin, J.J., Nenes,
605 A., Jonsson, H.H., Flagan, R.C. and Seinfeld, J.H.: Observations of continental
606 biogenic impacts on marine aerosol and clouds off the coast of California, *J. Geophys.*
607 *Res. Atmos.*, 119, 6724-6748, doi:10.1002/2013JD021228, 2014.

608 Collins, D. B., Ault, A. P., Moffet, R. C., Ruppel, M. J., Cuadra - Rodriguez, L. A.,
609 Guasco, T. L., Corrigan, C. E., Pedler, B. E., Azam, F., Aluwihare, L. I., Bertram, T.
610 H., Roberts, G. C., Grassian, V. H. and Bertram, T. H.: Impact of marine
611 biogeochemistry on the chemical mixing state and cloud forming ability of nascent sea
612 spray aerosol, *J. Geophys. Res. Atmos.*, 118(15), 8553-8565, 2013.

613 Cziczo, D.J., Murphy, D.M., Hudson, P.K. and Thomson, D.S.: Single particle
614 measurements of the chemical composition of cirrus ice residue during CRYSTAL-
615 FACE, *J. Geophys. Res. Atmos.*, 109, D04201, doi:10.1029/2003JD004032, 2004.

616 Cziczo, D.J., Froyd, K.D., Hoose, C., Jensen, E.J., Diao, M., Zondlo, M.A., Smith, J.B.,
617 Twohy, C.H. and Murphy, D.M.: Clarifying the dominant sources and mechanisms of
618 cirrus cloud formation, *Science*, 340, 1320-1324, doi: 10.1126/science.1234145, 2013.

619 Drewnick, F., Schneider, J., Hings, S. S., Hock, N., Noone, K., Targino, A., Weimer, S.
620 and Borrmann, S.: Measurement of ambient, interstitial, and residual aerosol particles
621 on a mountaintop site in central Sweden using an aerosol mass spectrometer and a CVI,
622 *J. Atmos. Chem.*, 56, 1-20, doi:10.1007/s10874-006-9036-8, 2007.

623 Deng, X., Wu, D., Shi, Y., Tang, H., Fan, S., Huang, H., Mao, W. and Ye, Y.:
624 Comprehensive analysis of the macro-and micro-physical characteristics of dense fog
625 in the area south of the Nanling Mountains (in Chinese), *J.Trop. Meteorol.*, 23, 424-
626 434, 2007.

627 Duncan, B. N., Martin, R. V., Staudt, A. C., Yevich, R. and Logan, J. A.: Interannual and
628 seasonal variability of biomass burning emissions constrained by satellite observations,
629 *J. Geophys. Res. Atmos.*, 108(D2), doi:108, 10.1029/2002jd002378, 2003.

630 Dusek, U., Frank, G., Hildebrandt, L., Curtius, J., Schneider, J., Walter, S., Chand, D.,
631 Drewnick, F., Hings, S. and Jung, D.: Size matters more than chemistry for cloud-
632 nucleating ability of aerosol particles, *Science*, 312, 1375-1378, 2006.

633 Ervens, B. and Volkamer, R.: Glyoxal processing by aerosol multiphase chemistry:
634 towards a kinetic modeling framework of secondary organic aerosol formation in
635 aqueous particles, *Atmos. Chem. Phys.*, 10(17), 8219-8244, 2010.

636 Facchini, M. C., Decesari, S., Rinaldi, M., Carbone, C., Finessi, E., Mircea, M., Fuzzi, S.,
637 Moretti, F., Tagliavini, E. and Ceburnis, D.: Important source of marine secondary
638 organic aerosol from biogenic amines, *Environ. Sci. Technol.*, 42, 9116-9121, doi:
639 10.1021/es8018385, 2008.

640 Furukawa, T. and Takahashi, Y.: Oxalate metal complexes in aerosol particles:
641 implications for the hygroscopicity of oxalate-containing particles, *Atmos. Chem.*
642 *Phys.*, 11, 4289-4301, doi:10.5194/acp-11-4289-2011, 2011.

643 Hallberg, A., Ogren, J. A., Noone, K. J., Okada, K., Heintzenberg, J. and Svenningsson, I.
644 B.: The influence of aerosol particle composition on cloud droplet formation, *J. Atmos.*
645 *Chem.*, 19, 153-171, doi: 10.1007/978-94-011-0313-8_8, 1994.

646 Harris, E., Sinha, B., van Pinxteren, D., Tilgner, A., Fomba, K. W., Schneider, J., Roth,
647 A., Gnauk, T., Fahlbusch, B. and Mertes, S.: Enhanced role of transition metal ion
648 catalysis during in-cloud oxidation of SO₂, *Science*, 340, 727-730,
649 doi:10.1126/science.1230911, 2013.

650 Harris, E., Sinha, B., van Pinxteren, D., Schneider, J., Poulain, L., Collett, J., D'Anna, B.,
651 Fahlbusch, B., Foley, S., Fomba, K. W., George, C., Gnauk, T., Henning, S., Lee, T.,
652 Mertes, S., Roth, A., Stratmann, F., Borrmann, S., Hoppe, P. and Herrmann, H.: In-
653 cloud sulfate addition to single particles resolved with sulfur isotope analysis during
654 HCCT-2010, *Atmos. Chem. Phys.*, 14, 4219-4235, doi:10.5194/acp-14-4219-2014,
655 2014.

656 Hammer, E., Gysel, M., Roberts, G.C., Elias, T., Hofer, J., Hoyle, C.R., Bukowiecki, N.,
657 Dupont, J.C., Burnet, F., Baltensperger, U. and Weingartner, E.: Size-dependent
658 particle activation properties in fog during the ParisFog 2012/13 field campaign,
659 *Atmos. Chem. Phys.*, 14, 10517-10533, 2014.

660 Hayden, K. L., Macdonald, A. M., Gong, W., Toom-Saunty, D., Anlauf, K. G., Leithead,
661 A., Li, S. M., Leaitch, W. R. and Noone, K.: Cloud processing of nitrate, *J. Geophys.*
662 *Res. Atmos.*, 113(D18), doi:10.1029/2007jd009732, 2008.

663 Herckes, P., Valsaraj, K.T. and Collett, J.L., A review of observations of organic matter
664 in fogs and clouds: Origin, processing and fate, *Atmos. Res.*, 132, 434-449. 2013.

665 Hiranuma, N., Brooks, S. D., Moffet, R. C., Glen, A., Laskin, A., Gilles, M. K., Liu, P.,
666 Macdonald, A.M., Strapp, J.W. and McFarquhar, G. M.: Chemical characterization of
667 individual particles and residuals of cloud droplets and ice crystals collected on board

668 research aircraft in the ISDAC 2008 study, *J. Geophys. Res. Atmos.*, 118(12), 6564-
669 6579, 2013.

670 Hudson, P.K., Murphy, D.M., Cziczo, D.J., Thomson, D.S., de Gouw, J.A., Warneke, C.,
671 Holloway, J., Jost, H.J. and Hübler, G.: Biomass-burning particle measurements:
672 Characteristic composition and chemical processing, *J. Geophys. Res. Atmos.*, 109,
673 D23S27, doi:10.1029/2003JD004398, 2004.

674 Kamphus, M., Ettner-Mahl, M., Klimach, T., Drewnick, F., Keller, L., Cziczo, D. J.,
675 Mertes, S., Borrmann, S. and Curtius, J.: Chemical composition of ambient aerosol, ice
676 residues and cloud droplet residues in mixed-phase clouds: single particle analysis
677 during the Cloud and Aerosol Characterization Experiment (CLACE 6), *Atmos. Chem.*
678 *Phys.*, 10, 8077-8095, doi:10.5194/acp-10-8077-2010, 2010.

679 Kleinman, L.I., Daum, P.H., Lee, Y.-N., Lewis, E.R., Sedlacek III, A., Senum, G.,
680 Springston, S., Wang, J., Hubbe, J. and Jayne, J.: Aerosol concentration and size
681 distribution measured below, in, and above cloud from the DOE G-1 during VOCALS-
682 Rex, *Atmos. Chem. Phys.*, 12, 207-223, 2012.

683 Laskin, A., Moffet, R. C., Gilles, M. K., Fast, J. D., Zaveri, R. A., Wang, B., Nigge P.
684 and Shutthanandan, J.: Tropospheric chemistry of internally mixed sea salt and organic
685 particles: Surprising reactivity of NaCl with weak organic acids, *J. Geophys. Res.*
686 *Atmos.*, 117(D15), doi:10.1029/2012JD017743, 2012.

687 Lee, C. S. L., Li, X., Zhang, G., Peng, X. and Zhang, L.: Biomonitoring of trace metals in
688 the atmosphere using moss (*Hypnum plumaeforme*) in the Nanling Mountains and the
689 Pearl River Delta, Southern China. *Atmos. Environ.*, 39(3), 397-407, 2005.

690 Li, L., Huang, Z., Dong, J., Li, M., Gao, W., Nian, H., Fu, Z., Zhang, G., Bi, X. and
691 Cheng, P.: Real time bipolar time-of-flight mass spectrometer for analyzing single
692 aerosol particles, *Int. J. Mass Spectrom.*, 303, 118-124,
693 doi:<http://dx.doi.org/10.1016/j.ijms.2011.01.017>, 2011a.

694 Li, T., Wang, Y., Zhou, J., Wang, T., Ding, A., Nie, W., Xue, L., Wang, X. and Wang,
695 W.: Evolution of trace elements in the planetary boundary layer in southern China:
696 effects of dust storms and aerosol-cloud interaction, *J. Geophys. Res. Atmos.*, 122,
697 3492-3506, 2017.

698 Li, W., Li, P., Sun, G., Zhou, S., Yuan, Q. and Wang, W.: Cloud residues and interstitial
699 aerosols from non-precipitating clouds over an industrial and urban area in northern
700 China, *Atmos. Environ.*, 45, 2488-2495, doi:[10.1016/j.atmosenv.2011.02.044](https://doi.org/10.1016/j.atmosenv.2011.02.044), 2011b.

701 Lohmann, U., Stier, P., Hoose, C., Ferrachat, S., Kloster, S., Roeckner, E. and Zhang, J.:
702 Cloud microphysics and aerosol indirect effects in the global climate model ECHAM5-
703 HAM, *Atmos. Chem. Phys.*, 7, 3425-3446, 2007.

704 Matsuki, A., Schwarzenboeck, A., Venzac, H., Laj, P., Crumeyrolle, S. and Gomes, L.:
705 Cloud processing of mineral dust: direct comparison of cloud residual and clear sky
706 particles during AMMA aircraft campaign in summer 2006, *Atmos. Chem. Phys.*, 10,
707 1057-1069, 2010.

708 McFiggans, G., Artaxo, P., Baltensperger, U., Coe, H., Facchini, M. C., Feingold, G.,
709 Fuzzi, S., Gysel, M., Laaksonen, A. and Lohmann, U.: The effect of physical and
710 chemical aerosol properties on warm cloud droplet activation, *Atmos. Chem. Phys.*, 6,
711 2593-2649, doi:[10.5194/acp-6-2593-2006](https://doi.org/10.5194/acp-6-2593-2006), 2006.

712 McMeeking, G. R., Good, N., Petters, M. D., McFiggans, G. and Coe, H.: Influences on
713 the fraction of hydrophobic and hydrophilic black carbon in the atmosphere, *Atmos.*
714 *Chem. Phys.*, 11(10), 5099-5112, 2011.

715 Medina, J., Nenes, A., Sotiropoulou, R. E. P., Cottrell, L. D., Ziemba, L. D., Beckman, P.
716 J. and Griffin, R. J.: Cloud condensation nuclei closure during the International
717 Consortium for Atmospheric Research on Transport and Transformation 2004
718 campaign: Effects of size-resolved composition, *J. Geophys. Res. Atmos.*, 112(D10S31),
719 doi:10.1029/2006JD007588, 2007.

720 Mertes, S., Lehmann, K., Nowak, A., Massling, A. and Wiedensohler, A.: Link between
721 aerosol hygroscopic growth and droplet activation observed for hill-capped clouds at
722 connected flow conditions during FEBUKO, *Atmos. Environ.*, 39, 4247-4256, 2005.

723 Moffet, R.C., Foy, B. D., Molina, L. A., Molina, M. and Prather, K.A.: Measurement of
724 ambient aerosols in northern Mexico City by single particle mass spectrometry, *Atmos.*
725 *Chem. Phys.*, 8, 4499-4516, doi:10.5194/acp-8-4499-2008, 2008.

726 Moffet, R.C. and Prather, K.A.: In-situ measurements of the mixing state and optical
727 properties of soot with implications for radiative forcing estimates, *Proc. Natl. Acad.*
728 *Sci. USA*, 106, 11872-11877, doi: 10.1073/pnas.0900040106, 2009.

729 Moore, K. F., Sherman, D. E., Reilly, J. E. and Collett, J. L.: Drop size-dependent
730 chemical composition in clouds and fogs. Part I. Observations, *Atmos. Environ.*,
731 38(10), 1389-1402, 2004.

732 Moteki, N., Adachi, K., Ohata, S., Yoshida, A., Harigaya, T., Koike, M. and Kondo, Y.:
733 Anthropogenic iron oxide aerosols enhance atmospheric heating, *Nature Commun.*, 8,
734 15329, doi: 10.1038/ncomms15329, 2017.

735 Pratt, K.A., DeMott, P.J., French, J.R., Wang, Z., Westphal, D.L., Heymsfield, A.J.,
736 Twohy, C.H., Prenni, A.J. and Prather, K.A.: In situ detection of biological particles in
737 cloud ice-crystals, *Nature Geos.*, 2, 398-401, 2009a.

738 Pratt, K.A., Hatch, L. E. and Prather, K. A.: Seasonal volatility dependence of ambient
739 particle phase amines, *Environ. Sci. Technol.*, 43, 5276-5281, doi:10.1021/es803189n,
740 2009b.

741 Pratt, K.A., Heymsfield, A. J., Twohy, C. H., Murphy, S. M., DeMott, P. J., Hudson, J.
742 G., Subramanian, R., Wang, Z., Seinfeld, J. H. and Prather, K. A.: In Situ Chemical
743 Characterization of Aged Biomass-Burning Aerosols Impacting Cold Wave Clouds, *J.*
744 *Atmos. Sci.*, 67, 2451-2468, doi:10.1175/2010jas3330.1, 2010a.

745 Pratt, K.A., Murphy, S., Subramanian, R., DeMott, P., Kok, G., Campos, T., Rogers, D.,
746 Prenni, A., Heymsfield, A. and Seinfeld, J.: Flight-based chemical characterization of
747 biomass burning aerosols within two prescribed burn smoke plumes, *Atmos. Chem.*
748 *Phys.*, 11, 12549-12565, doi:10.5194/acp-11-12549-2011, 2011.

749 Pratt, K.A., Twohy, C.H., Murphy, S.M., Moffet, R.C., Heymsfield, A.J., Gaston, C.J.,
750 DeMott, P.J., Field, P.R., Henn, T.R., Rogers, D.C., Gilles, M.K., Seinfeld, J.H. and
751 Prather, K.A.: Observation of playa salts as nuclei in orographic wave clouds, *J.*
752 *Geophys. Res. Atmos.*, 115, D15301, doi:10.1029/2009JD013606, 2010b.

753 Qin, X., Bhave, P.V. and Prather, K. A.: Comparison of two methods for obtaining
754 quantitative mass concentrations from aerosol time-of-flight mass spectrometry
755 measurements, *Anal. Chem.*, 78(17), 6169-6178, doi: 10.1021/ac060395q, 2006.

756 Rehbein, P. J., Jeong, C. H., McGuire, M. L., Yao, X., Corbin, J. C. and Evans, G. J.:
757 Cloud and fog processing enhanced gas-to-particle partitioning of trimethylamine,
758 Environ. Sci. Technol., 45, 4346-4352, doi:10.1021/es1042113, 2011.

759 Rosenfeld, D., Lohmann, U., Raga, G.B., O'Dowd, C.D., Kulmala, M., Fuzzi, S., Reissell,
760 A. and Andreae, M.O.: Flood or drought: how do aerosols affect precipitation?,
761 Science, 321, 1309-1313, doi: 10.1126/science.1160606, 2008.

762 Roth, A., Schneider, J., Klimach, T., Mertes, S., van Pinxteren, D., Herrmann, H. and
763 Borrmann, S.: Aerosol properties, source identification, and cloud processing in
764 orographic clouds measured by single particle mass spectrometry on a central
765 European mountain site during HCCT-2010, Atmos. Chem. Phys., 16, 505-524,
766 doi:10.5194/acp-16-505-2016, 2016.

767 Schneider, J., Mertes, S., van Pinxteren, D., Herrmann, H. and Borrmann, S.: Uptake of
768 nitric acid, ammonia, and organics in orographic clouds: Mass spectrometric analyses
769 of droplet residual and interstitial aerosol particles, Atmos. Chem. Phys., 17, 1571-
770 1593, doi:10.5194/acp-17-1571-2017, 2017.

771 Seinfeld, J.H., Bretherton, C., Carslaw, K.S., Coe, H., DeMott, P.J., Dunlea, E.J.,
772 Feingold, G., Ghan, S., Guenther, A.B. and Kahn, R.: Improving our fundamental
773 understanding of the role of aerosol-cloud interactions in the climate system, Proc. Natl.
774 Acad. Sci. USA, 113, 5781-5790, doi: 10.1073/pnas.1514043113, 2016.

775 Sellegri, Laj, P., Dupuy, R., Legrand, M., Preunkert, S. and Putaud, J.P.: Size-dependent
776 scavenging efficiencies of multicomponent atmospheric aerosols in clouds, J. Geophys.
777 Res. Atmos., 108, 4334, doi:10.1029/2002JD002749, 2003a.

778 Sellegri, K., Laj, P., Marinoni, A., Dupuy, R., Legrand, M. and Preunkert, S.:
779 Contribution of gaseous and particulate species to droplet solute composition at the
780 Puy de Dôme, France, *Atmos. Chem. Phys.*, 3, 1509-1522, doi:10.5194/acp-3-1509-
781 2003, 2003b.

782 Shingler, T., Dey, S., Sorooshian, A., Brechtel, F. J., Wang, Z., Metcalf, A., Coggon, M.,
783 Müllmenstädt, J., Russell, L. M., Jonsson, H. H. and Seinfeld, J. H.: Characterisation
784 and airborne deployment of a new counterflow virtual impactor inlet, *Atmos. Meas.*
785 *Tech.*, 5, 1259-1269, doi:10.5194/amt-5-1259-2012, 2012.

786 Sjogren, S., Gysel, M., Weingartner, E., Baltensperger, U., Cubison, M. J., Coe, H.,
787 Zardini, A.A., Marcolli, C., Krieger, U.K. and Krieger Peter, T.: Hygroscopic growth
788 and water uptake kinetics of two-phase aerosol particles consisting of ammonium
789 sulfate, adipic and humic acid mixtures, *J. Aerosol Sci.*, 38(2), 157-171, 2007.

790 Song, X.H., Hopke, P. K., Fergenson, D. P. and Prather, K. A.: Classification of single
791 particles analyzed by ATOFMS using an artificial neural network, ART-2A, *Anal.*
792 *Chem.*, 71, 860-865, doi:10.1021/ac9809682, 1999.

793 Sorooshian, A., Ng, N. L., Chan, A. W. H., Feingold, G., Flagan, R. C. and Seinfeld, J. H.:
794 Particulate organic acids and overall water-soluble aerosol composition measurements
795 from the 2006 Gulf of Mexico Atmospheric Composition and Climate Study
796 (GoMACCS), *J. Geophys. Res. Atmos.*, 112(D13), doi:10.1029/2007JD008537, 2007a.

797 Sorooshian, A., Lu, M. L., Brechtel, F. J., Jonsson, H., Feingold, G., Flagan, R. C. and
798 Seinfeld, J. H.: On the source of organic acid aerosol layers above clouds, *Environ. Sci.*
799 *Technol.*, 41, 4647-4654, doi: 10.1021/es0630442, 2007b.

800 Stier, P., Feichter, J., Kinne, S., Kloster, S., Vignati, E., Wilson, J., Ganzeveld, L., Tegen,
801 I., Werner, M. and Balkanski, Y.: The aerosol-climate model ECHAM5-HAM, *Atmos.*
802 *Chem. Phys.*, 5, 1125-1156, 2005.

803 Svenningsson, B., Rissler, J., Swietlicki, E., Mircea, M., Bilde, M., Facchini, M. C.,
804 Decesari, S., Fuzzi, S., Zhou, J., Mønster, J. and Rosenørn, T.: Hygroscopic growth
805 and critical supersaturations for mixed aerosol particles of inorganic and organic
806 compounds of atmospheric relevance, *Atmos. Chem. Phys.*, 6(7), 1937-1952, 2006.

807 Tang, M., Cziczo, D. J. and Grassian, V. H.: Interactions of Water with Mineral Dust
808 Aerosol: Water Adsorption, Hygroscopicity, Cloud Condensation, and Ice Nucleation,
809 *Chem. Rev.*, doi:10.1021/acs.chemrev.5b00529, 2016.

810 Targino, A.C., Krejci, R., Noone, K.J. and Glantz, P.: Single particle analysis of ice
811 crystal residuals observed in orographic wave clouds over Scandinavia during
812 INTACC experiment, *Atmos. Chem. Phys.*, 6, 1977-1990, 2006.

813 Tsai, J.H., Lin, K.H., Chen, C.Y., Ding, J.Y., Choa, C.G. and Chiang, H.L.: Chemical
814 constituents in particulate emissions from an integrated iron and steel facility, *J.*
815 *Hazard. Mater.*, 147, 111-119, 2007.

816 Twohy, C.H., Kreidenweis, S.M., Eidhammer, T., Browell, E.V., Heymsfield, A.J.,
817 Bansemer, A.R., Anderson, B.E., Chen, G., Ismail, S., DeMott, P.J. and Van Den
818 Heever, S.C.: Saharan dust particles nucleate droplets in eastern Atlantic clouds,
819 *Geophys. Res. Lett.*, 36, doi: 10.1029/2008GL035846, 2009.

820 Twohy, C.H. and Poellot, M.: Chemical characteristics of ice residual nuclei in anvil
821 cirrus clouds: evidence for homogeneous and heterogeneous ice formation, *Atmos.*
822 *Chem. Phys.*, 5, 2289-2297, 2005.

823 Twohy C.H. and Anderson J. R.: Droplet nuclei in non-precipitating clouds: composition
824 and size matter. *Environ. Res. Lett.*, 3, 045002, doi:10.1088/1748-9326/3/4/045002,
825 2008.

826 Wang, H., An, J., Shen, L., Zhu, B., Xia, L., Duan, Q. and Zou, J.: Mixing state of
827 ambient aerosols in Nanjing city by single particle mass spectrometry, *Atmos. Environ.*,
828 132, 123-132, 2016.

829 Wang, Y., Guo, J., Wang, T., Ding, A., Gao, J., Zhou, Y., Collett, J. L. and Wang, W.:
830 Influence of regional pollution and sandstorms on the chemical composition of
831 cloud/fog at the summit of Mt. Taishan in northern China, *Atmos. Res.*, 99, 434-442,
832 doi:10.1016/j.atmosres.2010.11.010, 2011.

833 Wiedensohler, A., Cheng, Y. F., Nowak, A., Wehner, B., Achtert, P., Berghof, M.,
834 Birmili, W., Wu, Z. J., Hu, M., Zhu, T., Takegawa, N., Kita, K., Kondo, Y., Lou, S. R.,
835 Hofzumahaus, A., Holland, F., Wahner, A., Gunthe, S. S., Rose, D., Su, H. and
836 Takegawa, N.: Rapid aerosol particle growth and increase of cloud condensation
837 nucleus activity by secondary aerosol formation and condensation: A case study for
838 regional air pollution in northeastern China, *J. Geophys. Res. Atmos.*, 114(D2),
839 doi:10.1029/2008JD010884, 2009.

840 Wise, M. E., Surratt, J. D., Curtis, D. B., Shilling, J. E. and Tolbert, M. A. Hygroscopic
841 growth of ammonium sulfate/dicarboxylic acids, *J. Geophys. Res. Atmos.*, 108(D20),
842 doi:10.1029/2003JD003775, 2003.

843 Zelenyuk, A., Imre, D., Earle, M., Easter, R., Korolev, A., Leitch, R., Liu, P.,
844 Macdonald, A. M., Ovchinnikov, M. and Strapp, W.: In Situ Characterization of Cloud
845 Condensation Nuclei, Interstitial, and Background Particles Using the Single Particle

846 Mass Spectrometer, SPLAT II†, *Anal. Chem.*, 82, 7943-7951, doi:10.1021/ac1013892,
847 2010.

848 Zhang, R.Y., Khalizov, A. F., Pagels, J., Zhang, D., Xue, H. and McMurry, P. H.:
849 Variability in morphology, hygroscopicity, and optical properties of soot aerosols
850 during atmospheric processing, *Proc. Natl. Acad. Sci. USA*, 105, 10291-10296,
851 doi:10.1073/pnas.0804860105, 2008.

852 Zhang, G., Bi, X., Chan, L. Y., Li, L., Wang, X., Feng, J., Sheng, G., Fu, J., Li, M. and
853 Zhou, Z.: Enhanced trimethylamine-containing particles during fog events detected by
854 single particle aerosol mass spectrometry in urban Guangzhou, China, *Atmos. Environ.*,
855 55, 121-126, doi:10.1016/j.atmosenv.2012.03.038, 2012a.

856 Zhang, G., Bi, X., Li, L., Chan, L. Y., Li, M., Wang, X., Sheng, G., Fu, J. and Zhou, Z.:
857 Mixing state of individual submicron carbon-containing particles during spring and fall
858 seasons in urban Guangzhou, China: a case study, *Atmos. Chem. Phys.*, 13, 4723-4735,
859 doi:10.5194/acp-13-4723-2013, 2013.

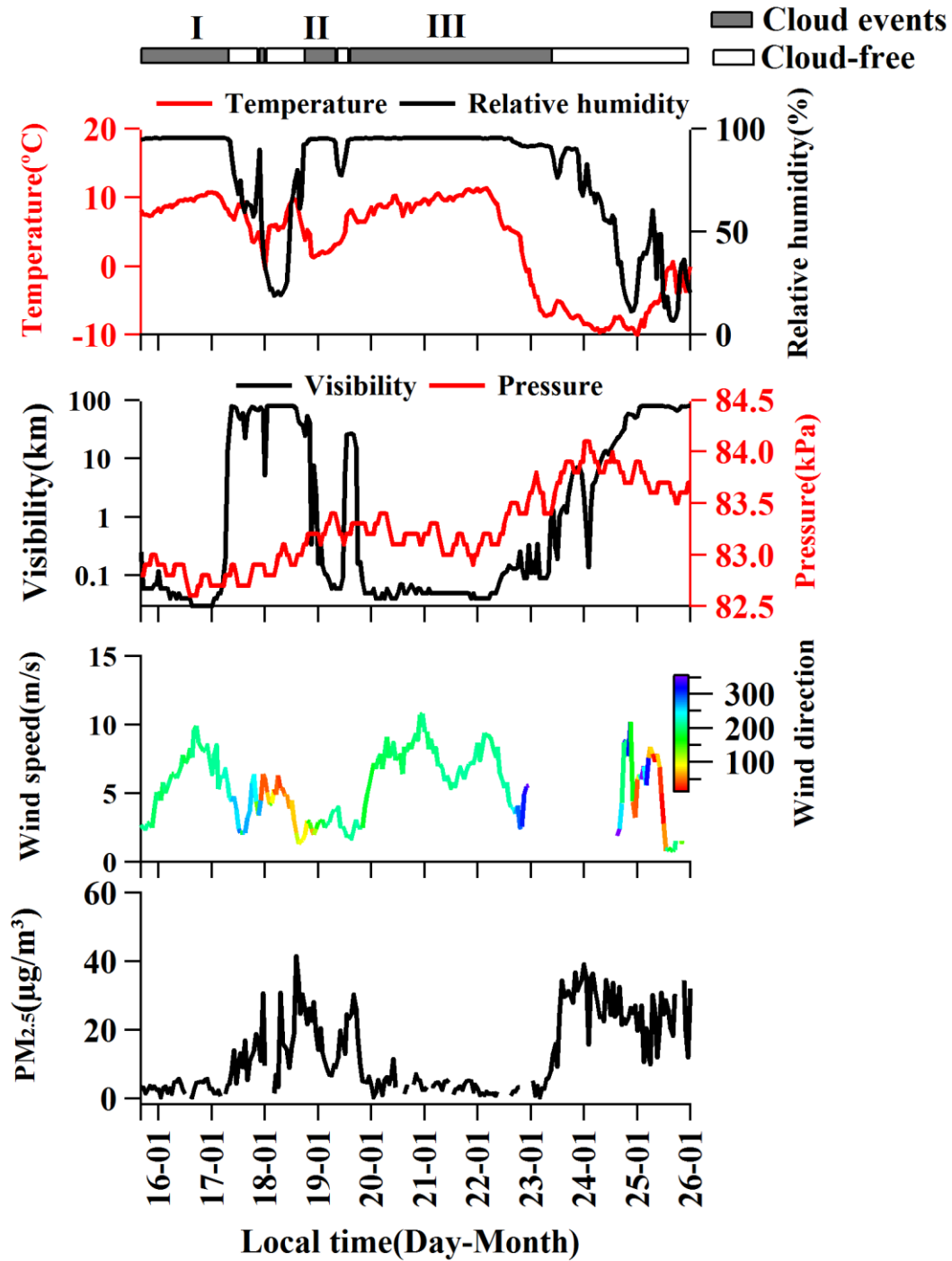
860 Zhang, G., Bi, X., Lou, S., Li, L., Wang, H., Wang, X., Zhou, Z., Sheng, G., Fu, J. and
861 Chen, C.: Source and mixing state of iron-containing particles in Shanghai by
862 individual particle analysis, *Chemosphere*, 95, 9-16, 2014.

863 Zhang, G., Lin, Q., Peng, L., Bi, X., Lei, M., Chen, D., Brechtel, F.J., Chen, X., Yan,
864 W., Wang, X., Peng, P., Sheng, G. and Zhou, Z.: Single particle mixing state and
865 cloud scavenging of black carbon at a high-altitude mountain site in south China, *J.*
866 *Geophys. Res. Atmos.*, in revise, 2017.

867 Zhang, X., Wang, Y., Niu, T., Zhang, X., Gong, S., Zhang, Y. and Sun, J.: Atmospheric
868 aerosol compositions in China: spatial/temporal variability, chemical signature,

869 regional haze distribution and comparisons with global aerosols, *Atmos. Chem. Phys.*,
870 12, 779-799, doi:10.5194/acp-12-779-2012, 2012b.

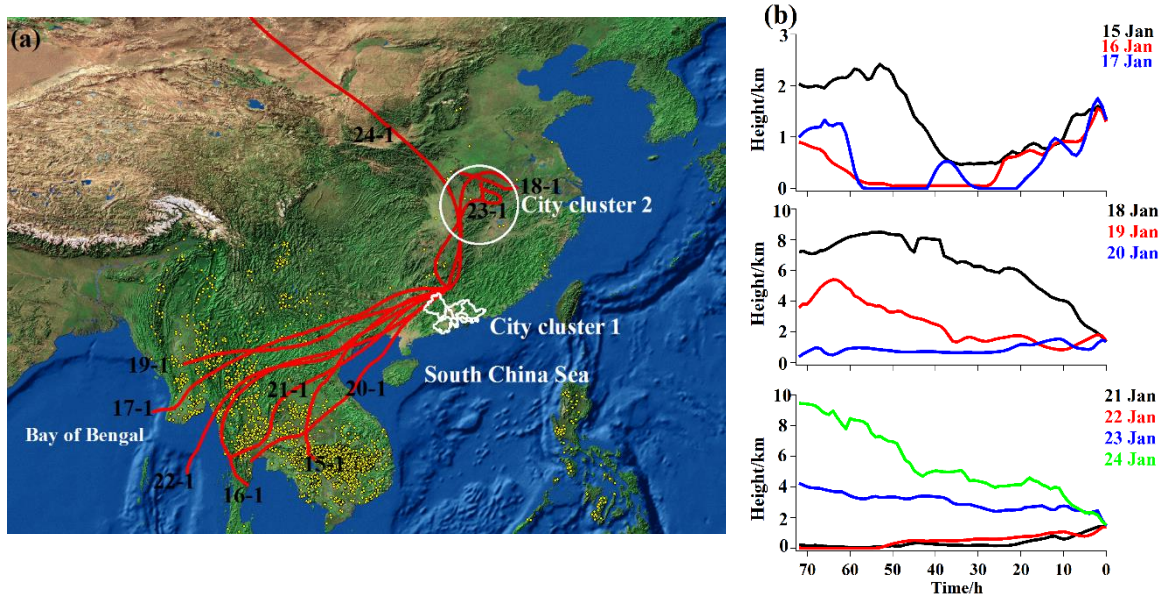
871 Zhang, Y.P., Wang, X.F., Chen, H., Yang, X., Chen, J.M. and Allen, J.O.: Source
872 apportionment of lead-containing aerosol particles in Shanghai using single particle
873 mass spectrometry, *Chemosphere*, 74, 501-507, 2009.



875

876 Figure 1: The hourly average variations in meteorological conditions (temperature,
 877 relative humidity, visibility, pressure, wind speed and direction) and PM_{2.5}.

878



879

880

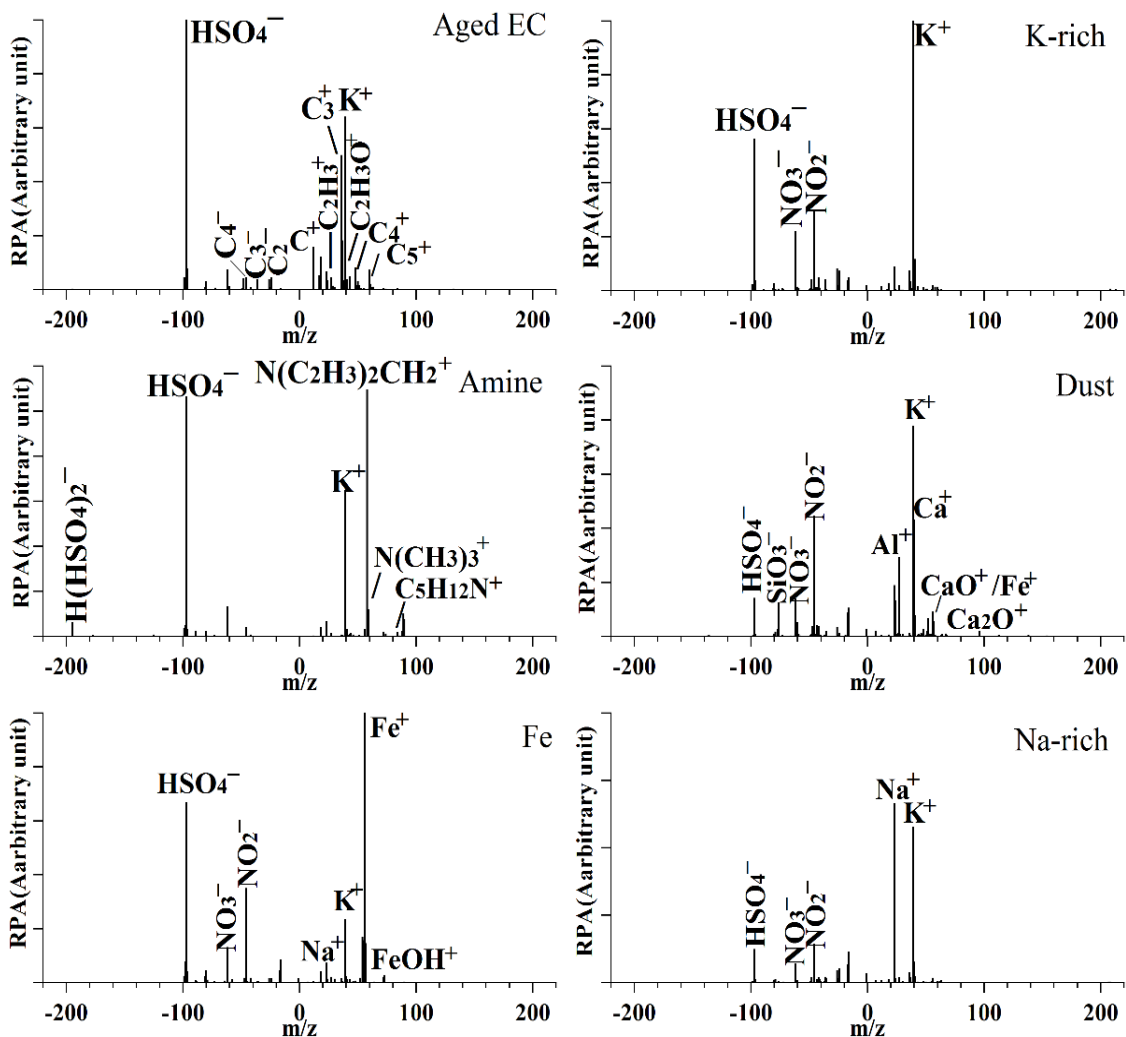
881 Figure 2: (a) HYSPLIT back trajectories (72 h) for air masses at 1,800 m during the

882 whole sampling period. The white borders and circle refer to the Pearl River Delta (city

883 cluster 1) and Yangtze River Mid-Reaches city clusters (city cluster 2), respectively. The

884 fire date (yellow dots) are available at <https://earthdata.nasa.gov/>; (b) Heights (above

885 model ground) of the air masses as a function of time.



886

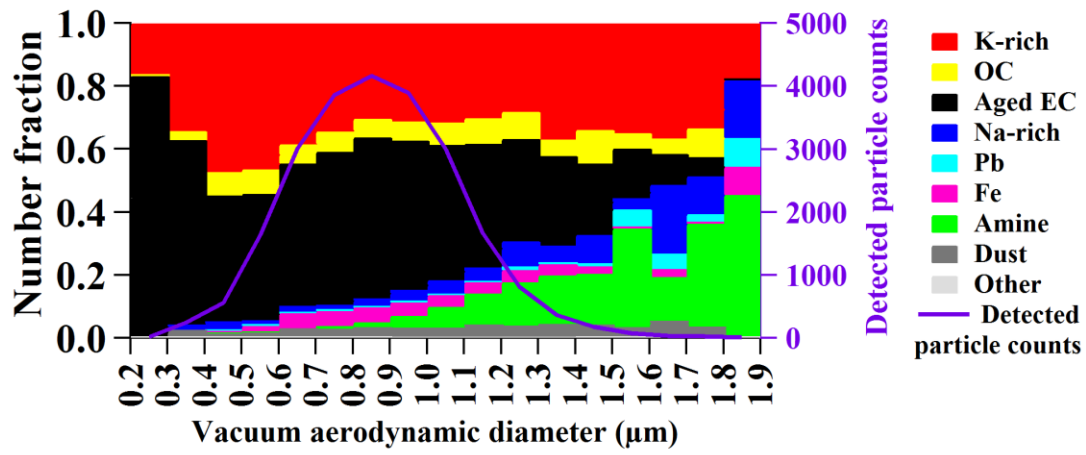
887

888 Figure 3: Averaged positive and negative mass spectra for the main 6 particle types

889 (Aged EC, K-rich, Amine, Dust, Fe, Na-rich) of the sampled particles. RPA in the

890 vertical axis refers to relative peak area. m/z in the horizontal axis represents mass-to-

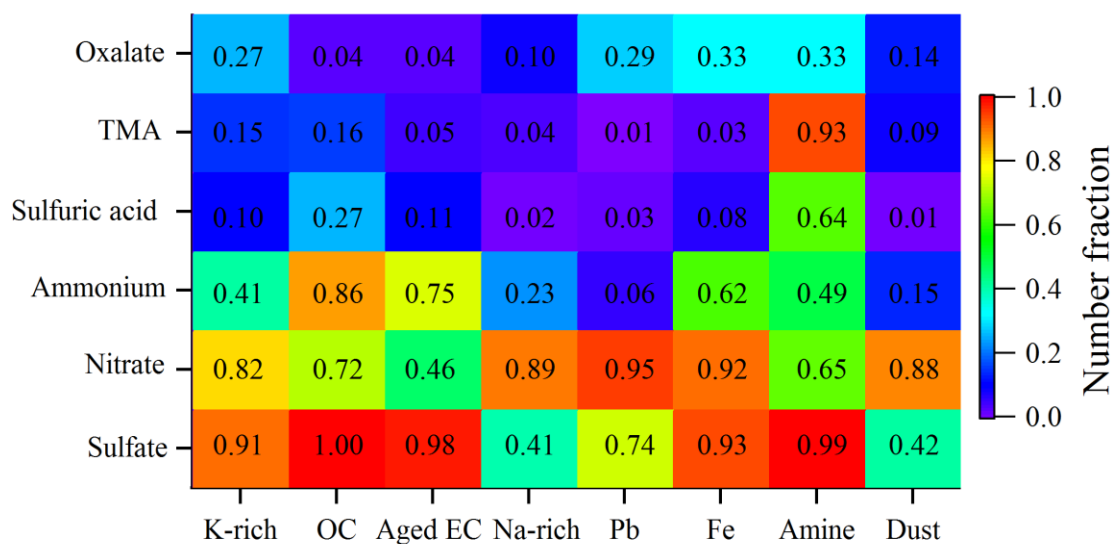
891 charge ratio.



892

893 Figure 4: Number fraction for size distribution of the cloud residual types in 100 nm size

894 intervals.



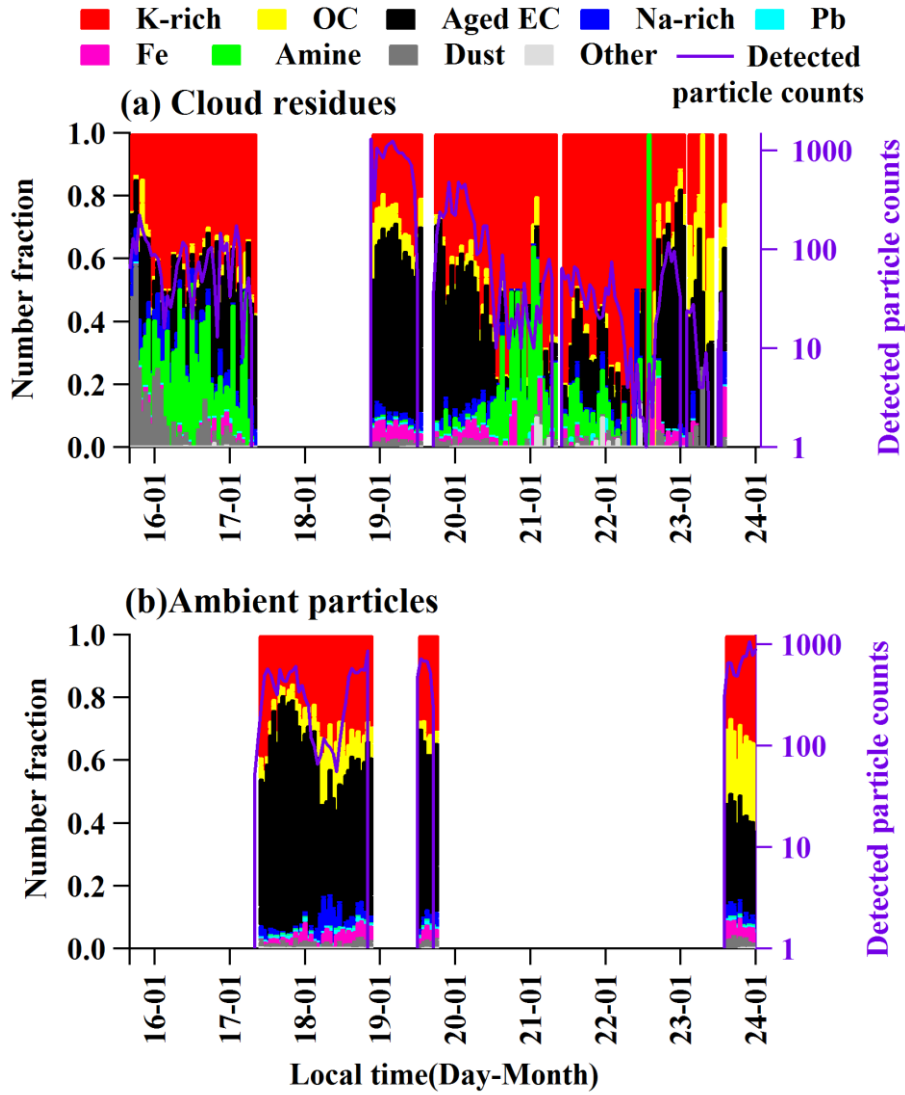
895

896 Figure 5: Number fraction of secondary markers associated with the total cloud residues

897 types; Sulfate (m/z , -97HSO_4^-), Nitrate (m/z , -46NO_2^- or -62NO_3^-), Ammonium (m/z ,

898 18NH_4^+), Sulfuric acid (m/z , $-195\text{H}(\text{HSO}_4)_2^-$), TMA (m/z , $59\text{N}(\text{CH}_3)_3^+$), Oxalate (m/z ,

899 $89\text{HC}_2\text{O}_4^-$).



900

901

902 Figure 6: The hourly average variations in the cloud residual and ambient particles during

903 the whole sampling period.

904

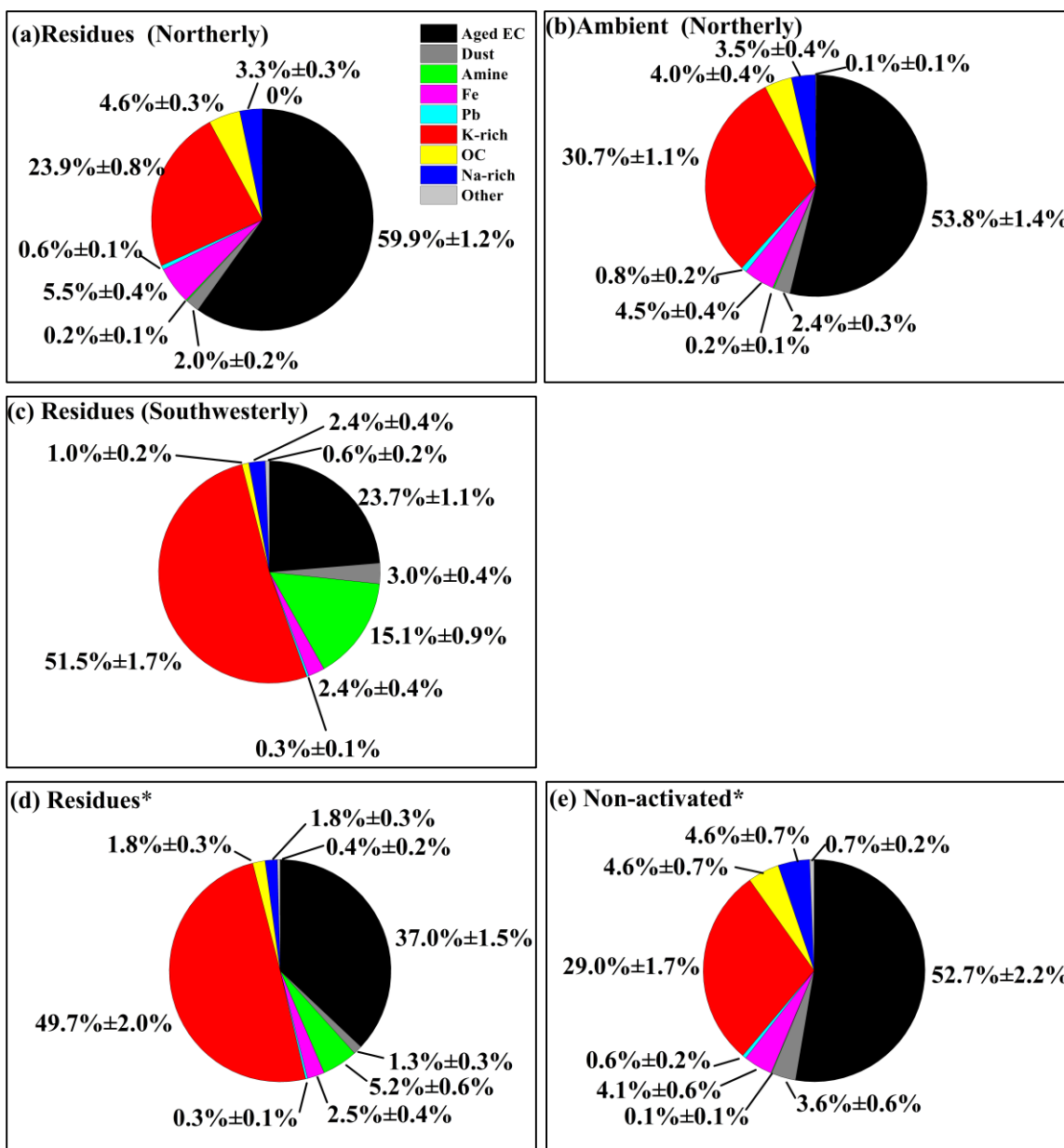
905

906

907

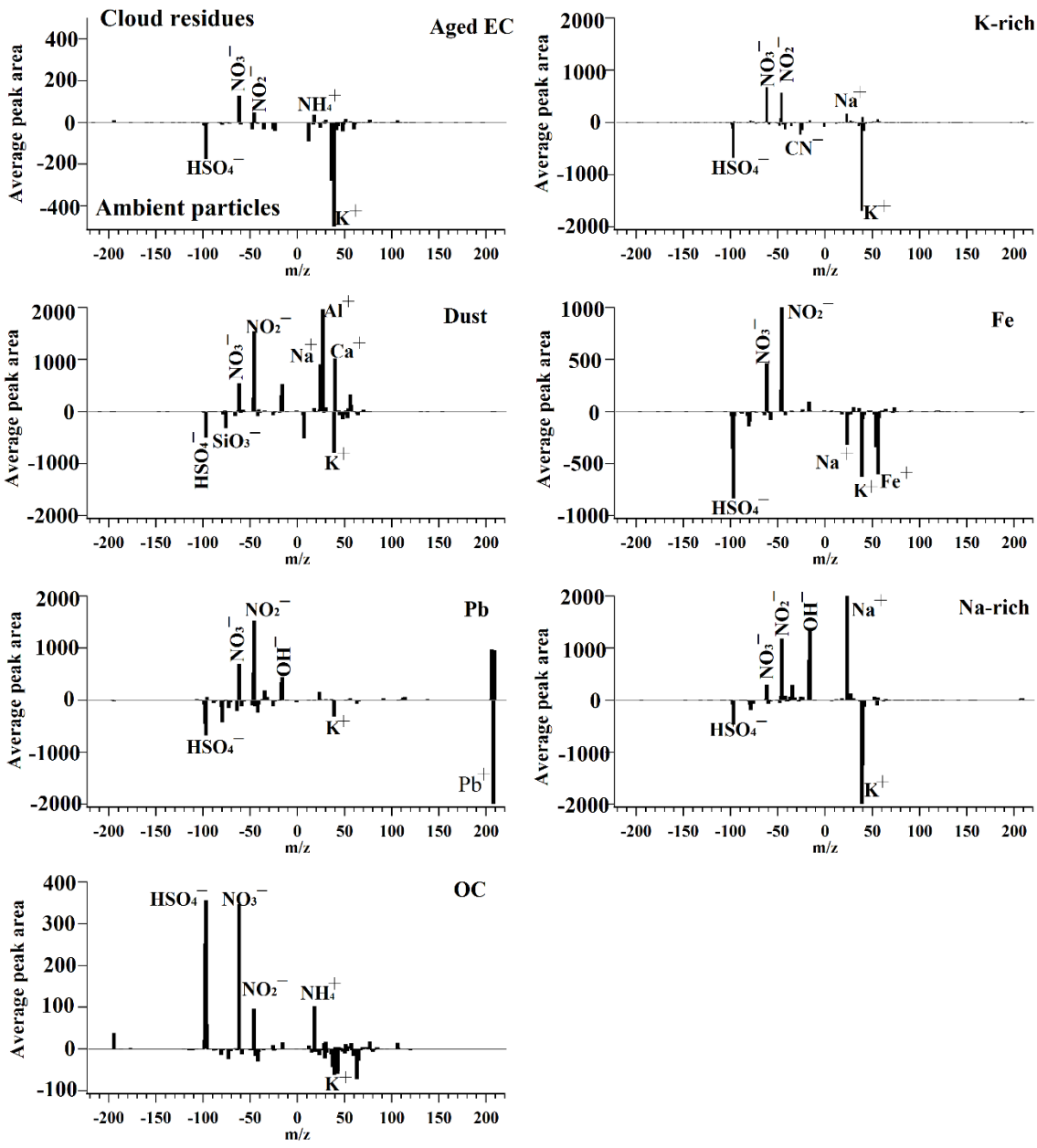
908

909



910

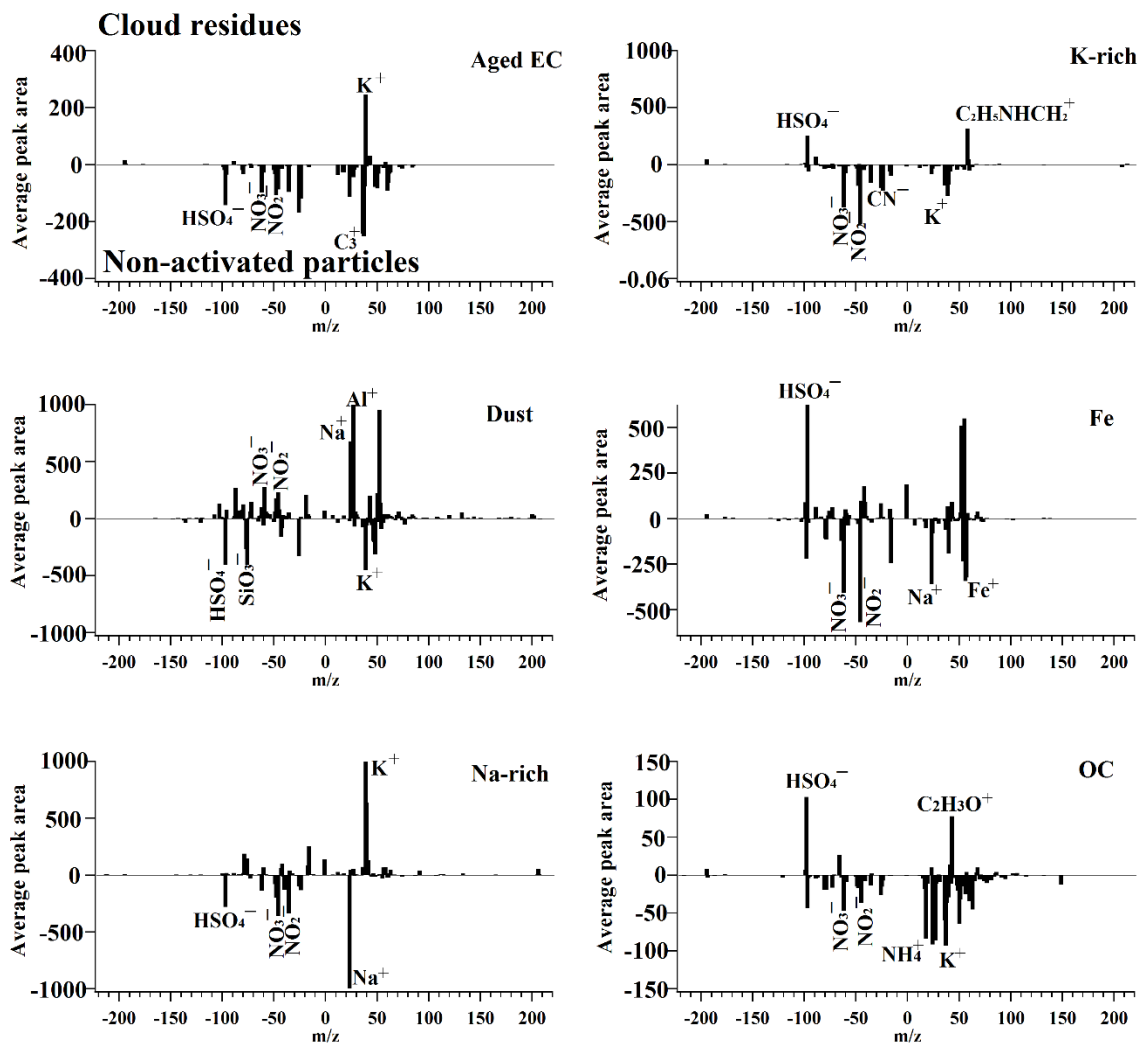
911 Figure 7: Number fraction of the cloud residues, ambient and non-activated particles. (a)
 912 cloud residues during northerly air mass; (b) ambient particle during northerly air mass;
 913 (c) cloud residues during southwesterly air mass; (d) cloud residues and (e) non-activated
 914 particles were alternately sampled with an interval of one hour during cloud III event.
 915 Uncertainties were calculated assuming Poisson statistics for analyzed particles.



916

917

918 Figure 8: Mass spectral subtraction plot of the average mass spectrum corresponding to
 919 cloud residues minus ambient particles. Positive area peaks correspond to higher
 920 abundance in cloud residues, whereas negative area peaks show higher intensity in
 921 ambient particles.



922
923

924 Figure 9: Mass spectral subtraction plot of the average mass spectrum corresponding to
925 cloud residues minus non-activated particles. Positive area peaks correspond to higher
926 abundance in cloud residues, whereas negative area peaks show higher intensity in non-
927 activated particles.